Growth yields and light-capture in PhycoCyanin and PhycoErythrin-rich picocyanobacteria, across photic regimes and growth phases

Sylwia Śliwińska-Wilczewska[1,2], Marta Konik[3,4], Mireille Savoie[1], Anabella Aguilera[5,6], Naaman M. Omar[1], and Douglas A. Campbell[1,*]

[1] Department of Biology, Mount Allison University, 53 York St., Sackville, NB, E4L 1C9, Canada

[2] Institute of Oceanography, University of Gdansk, 46 Pilsudskiego St, P81-378, Gdynia, Poland

[3] Department of Geography, University of Victoria, Victoria, BC, V8P 5C2, Canada

[4] Institute of Oceanology, Polish Academy of Sciences, 81-712 Sopot, Poland

[5] Department of Biology and Environmental Science, Centre for Ecology and Evolution in Microbial Model Systems (EEMiS), Linnaeus University, Kalmar, Sweden

[6] Department of Aquatic Sciences and Assessment, Swedish University of Agricultural Sciences, Uppsala, Sweden (present address)

[*] Correspondence: Douglas A. Campbell <dubhglascambeuil@gmail.com>

Running head: *Picocyanobacteria across photic regimes*

Abstract

The genus *Synechococcus* occurs from tropical to arctic zones, with climate scenarios forecasting range expansions of this picocyanobacteria into new photic regimes. We found that coastal PhycoCyanin(PC)-rich and PhycoErythrin(PE)-rich *Synechococcus* strains grew fastest under moderate photosynthetically active radiation, and a 24-hour photoperiod, despite a cumulative diel photon dose equivalent to conditions where growth was slower, under higher light and shorter photoperiods. Under optimal conditions, a PE-rich *Synechococcus* sp. achieved a highest recorded cyanobacterial chlorophyll-specific exponential growth rate of 4.5 d^{-1}. PE-rich strains demonstrated wider ability to modulate light capture capacity, whereas PC-rich strains showed less change in light capture across increasing cumulative diel photon dose. We found the coastal picocyanobacteria show consistent patterns of an exponential decay of effective absorption cross section for PSII photochemistry, versus increasing cumulative diel PAR doses. Effective absorption cross section for PSII excited through phycobilisome absorbance at 590 nm was positively correlated with phycobiliprotein:Chl *a*, particularly during pre-stationary growth phase. Within each strain, µ showed consistent saturating responses to increasing cumulative diel PSII electron flux. As photoperiod opportunists, coastal picocyanobacteria show potential to expand into longer photic regimes at warming higher latitudes.

Introduction

The photic regime, comprised of Photosynthetically Active Radiation (PAR), spectral quality, and photoperiod, is a pivotal influence on the growth and productivity of phytoplankton within aquatic ecosystems. PAR refers to the spectral range of solar radiation, approximately 400-700 nm, that is capable of driving photosynthesis. The availability and distribution of PAR

44   in aquatic ecosystems is influenced by cloud cover, water depth, and light attenuation due to

45   water turbidity and suspended particles, including phytoplankton cells (Field et al. 1998;

46   Torremorell et al. 2009). Photosynthetically Usable Radiation (PUR), in turn is the fraction of

47   PAR that can be absorbed for photosynthesis by pigments of a given cyanobacteria or algae

48   (Morel 1978). PUR thus depends upon the interaction of PAR, and the phytoplankter expression

49   of genomic capacities for light capture (Moejes et al. 2017). Cyanobacteria also respond to

50   changes in photoperiod, which serves as a key environmental cue for photosynthesis, growth,

51   reproduction, and nutrient assimilation (LaRoche and Robicheau 2022). Thus, in polar regions,

52   characterized by prolonged periods of wintertime darkness and continuous daylight during

53   summer, cyanobacteria encounter unique challenges. Light is the primary limitation on biomass

54   production in winter, suppressing cyanobacteria growth and metabolic activity, whereas

55   extended daylight in summer boosts photosynthetic activity (Arrigo 2014). In temperate regions,

56   seasonal variation in light-limitation is less pronounced, but cyanobacteria are still influenced by

57   daily and seasonal fluctuations, with a contrast between more favorable conditions for

58   cyanobacteria growth in spring and summer, compared to fall and winter (Huisman et al. 2002;

59   Holtrop et al. 2021). In the tropics, daylight hours remain nearly constant throughout the year

60   (Behrenfeld et al. 2006), and cyanobacteria productivity is rather controlled by nutrients

61   resupplied into the euphotic zone (Li et al. 2015), and mortality through viral lysis (Ortmann et

62   al. 2002) and zooplankton grazing (Christaki et al. 1999).

63   *Synechococcus*, a diverse genus of picocyanobacteria, exhibits a distribution spanning

64   diverse geographical regions (Flombaum et al. 2013), with strains demonstrating a remarkable

65   range of adaptations to environmental conditions (Śliwińska-Wilczewska et al. 2018a; Aguilera

66   et al. 2023). *Synechococcus* capacities to thrive across diverse marine and freshwater habitats

67   positions it as a pivotal agent in energy and nutrient transfer within food webs, connecting the

68   microbial loop with higher trophic levels, offering direct sustenance to grazers, including

69   zooplankton and small fish (Li 1995). As one of the two dominant picocyanobacterial genera in

70   oceanic waters, *Synechococcus* contribute significantly to light attenuation and light availability

71   for other photosynthetic marine organisms, thereby influencing ocean colour and allowing

72   satellite detection of *Synechococcus*-rich communities (Xi et al. 2020). General relations among

73   optical absorption spectra and pigment compositions have been used to determine diagnostic

74   pigment indices of major phytoplankton functional types (Hirata et al. 2011). Modeling suggests

75   that *Synechococcus* abundance and ranges will increase due to climate warming (Flombaum et

76   al. 2013). The projected changes may vary geographically and may include shifts in the spatial

77   distribution of the main picocyanobacteria, as well as changes in the proportions among

78   *Synechococcus* sp. lineages (Six et al. 2021), potentially pushing lineages into new photic

79   regimes. Synechococcus exhibits significant phenotypic diversity across lineages, encompassing

80   strains rich in phycobiliprotein pigments, phycoerythrin (PE-rich) or phycocyanin (PC-rich)

81   (Haverkamp et al. 2009; Aguilera et al. 2023). Phycobiliprotein pigments are pivotal for light

82   absorption during photosynthesis and confer distinctive colours to the picocyanobacteria (Stomp

83   et al. 2007). The disparate light preferences between PC-rich and PE-rich *Synechococcus* sp.

84   strains influence their ecological niches. PC-rich strains thrive in environments with elevated

85   light levels, such as surface waters and coastal regions. PE-rich strains exhibit adaptation to

86   lower-light conditions, primarily inhabiting the deeper layers of the water column. PC-rich and

87   PE-rich *Synechococcus* sp. strains thus predominantly occupy complementary habitats (Six et al.

88   2007; Haverkamp et al. 2009; Six et al. 2021), although differential responses of *Synechococcus*

89 lineages to photoperiod, have not been studied in detail, except for thermophilic PC-rich

90 *Synechococcus* PCC 6715 (Klepacz-Smółka et al. 2020).

91   Cyanobacteria growth includes lag, exponential growth, stationary, and death phases

92 (Reynolds 2006). During the lag phase, cyanobacteria acclimate to the environment and prepare

93 for active growth by synthesizing essential cellular components. Exponential growth phase is

94 marked by cell division and biomass accumulation, fueled by nutrient and light availability. If

95 growth is limited by declining nutrients, by light, or by accumulation of inhibitory factors, algae

96 enter stationary phase, characterized by a balance between cell division and death, leading to a

97 plateau in population. The death phase occurs when cyanobacteria cell death outruns division,

98 leading to net decomposition, contributing to nutrient recycling in aquatic ecosystems (Reynolds

99 2006). Moreover, Schuurmans et al. (2017) proposed an additional phase between the

100 exponential and stationary phases of picocyanobacteria growth, which is often neglected in

101 physiological studies. Herein, we examined the physiological responses of PC-rich and PE-rich

102 *Synechococcus* sp. in this phase, which we termed the pre-stationary phase of growth.

103   Picocyanobacteria are the most abundant phytoplankters in aquatic ecosystems and are

104 crucial to the optical properties of ocean water, by influencing its colour and transparency. PC-

105 rich and PE-rich *Synechococcus* sp. may have different costs and physiological strategies for

106 growth under different photic regimes, which could drive spatial and temporal variability of

107 picocyanobacteria biomass and community composition, in current and potential future aquatic

108 habitats. Therefore, our aim was to determine whether photic regimes and growth phases

109 differentially affect growth and light-capture, between representative PC-rich and PE-rich

110 *Synechococcus* sp.

111

Materials and Methods

Experimental setup

Two xenic PhycoCyanin(PC)-rich (CCBA_056 or CCBA_077) strains and two

PhycoErythrin(PE)-rich (CCBA_048 or CCBA_127) strains of *Synechococcus* were obtained

from the Culture Collection of Baltic Algae (CCBA; https://ccba.ug.edu.pl/pages/en/home.php).

Pre-cultures of picocyanobacteria strains were maintained in Tissue Culture Flasks (VWR

International, Cat. No. 10062-872, PA, USA) and were transferred to fresh f/2 media (Guillard

1975) at salinity of 8 PSU (which corresponds to their natural habitat) every two weeks, under a

photoperiod of 12 h and Photosynthetically Active Radiation (PAR) of 10 µmol photons $m^{-2}s^{-1}$

supplied from cool white fluorescent tubes, at 22°C.

Experimental cultures of each strain were grown in 8 x 80 mL round bottom cylindrical

glass tubes in a Multi-Cultivator MC 1000-OD (Photon Systems Instruments, Drásov, Czech

Republic). Each culture tube contained 75 mL of f/2 medium inoculated with 5 mL of growing

pre-culture, to achieve exponential growth from the beginning of the experiment, with little to no

lag phase upon inoculation. Culture tubes were inoculated in the afternoon while the

photoregime of a sinuisoidal photoperiod commenced the following morning such that peak PAR

occurred at noon each day.

Cultures grew at 22°C, with photoperiods of 8, 12, 16, or 24 h, with peak PAR of 30, 90,

180, 300, 600, or 900 µmol photons $m^{-2}s^{-1}$ independently supplied to each culture tube from

white LED lamps. To approximate diel cycles, the photoperiods of 8 – 16 h were applied in a

sinuisoidal shape, while the 24-hour photoperiod was applied continuously in a square shape.

The area under the sinuisoidal curve is 1/2 the area under a square of equal width, therefore at

134   equivalent peak PAR the 24 h square photoperiod cultures received 4 times the diel photon doses

135   of the 12 h sinuisoidal photoperiod cultures.

136   Culture tubes were closed with a silicone inert silicone stopper perforated by an aeration

137   input tube extending to the bottom of the culture tube, and a pressure outlet tube. Aeration with a

138   total air flow rate of around ~ 140 mL min^{-1} tube^{-1} through a 0.2µm filter ensured mixing and

139   provided sufficient air/CO_2 supply to cultures through the entire culture volume. The pH of

140   tested cultures did not fluctuate fiercely during the experiment and remained at approximately 8

141   – 9. Light, temperature, optical density, and aeration gas of the Multi-Cultivator system were

142   monitored and controlled via the Photobioreactor Control Software (Photon Systems

143   Instruments, Drásov, Czech Republic).

144

DNA extractions

146   Samples for total genomic DNA were collected by harvesting 10 mL of each culture and

147   centrifuging for 8 minutes at 8,000 x. DNA was extracted using the FastDNA™ SPIN Kit for

148   Soil (MP Biomedicals) with Matrix E columns following manufacturer instructions with the

149   addition of an incubation with proteinase-K (1% final concentration) at 55°C for one hour. DNA

150   concentration was measured using an Invitrogen Qubit 2.0 fluorometer (Thermo Fisher Scientific

151   Inc.) and purity was assessed using a Thermo Scientific™ NanoDrop 2000 spectrophotometer

152   (Thermo Fisher Scientific Inc.).

153   The phylogenetic placement of CCBA strains (Fig. S1 in Supporting Information) within

154   cluster 5 picocyanobacteria was explored by amplifying and sequencing a fragment of the 16S

155   rRNA gene using universal primers 27F and 1492R (Lane 1991). 16S rRNA gene sequences

156   were aligned with MAFFT v. 7.5 using the G-INS-I algorithm (Katoh et al. 2019). Phylogenetic

157   trees were created using IQ-TREE v. 1.6.12 (Hoang et al. 2018), using GTR+F+I+I+R3 model

158   determined by ModelFinder (Kalyaanamoorthy et al. 2017). Bootstrap values were calculated

159   with 1000 replicates (Hoang et al. 2018).

160

Growth curves and chlorophyll-specific exponential growth rates

162   Picocyanobacterial growth was monitored every 5 minutes by automatically recording

163   OD_{680}, OD_{720}, and ΔOD ($\Delta OD = OD_{680} - OD_{720}$) for 14 days, independently for each culture

164   tube. The exceptions were experiments conducted with a photoperiod of 24 h and light of 600 or

165   900 µmol photons $m^{-2}s^{-1}$, which lasted 7 days (Fig. S2). The chlorophyll-specific exponential

166   growth rates (µ) were determined by fitting logistic growth curves using a modified Levenberg-

167   Marquardt fitting algorithm (Elzhov et al. 2023) to plots of the chlorophyll *a* proxy of ΔOD

168   vs. elapsed time for each combination of strain, photoperiod, and peak PAR (Fig. S3).

169   To summarize the growth responses of the four picocyanobacterial strains we used a

170   Generalized Additive Model (GAM) (Wood 2017) was applied to the relation of chlorophyll-

171   specific µ, d^{-1} to photoperiod and PAR level. The R package *mgcv* (Wood 2017) was used to

172   model the growth rate with smoothing terms and indicate the 90, 50 and 10% quantiles for

173   growth rate across the levels of factors. Only growth rate estimates for which the amplitude of

174   standard error was smaller than 50% of the fitted growth rate were included in the GAM. We

175   visually compared the GAM contours to isoclines of equal cumulative diel PAR (µmol photons

176     $m^{-2}d^{-1}$).

177   The 1st derivative of OD_{680} taken over 1 h increments was computed using *xts*: eXtensible

178   Time Series (Ryan et al. 2024) and *signal*: Signal Processing (Ligges et al. 2024) R packages.

179   The time when the cultures reached their maximum absolute hourly growth (tMaxAHG) of the

180   1st derivative of OD_{680} was taken as the time of transition from exponential to pre-stationary
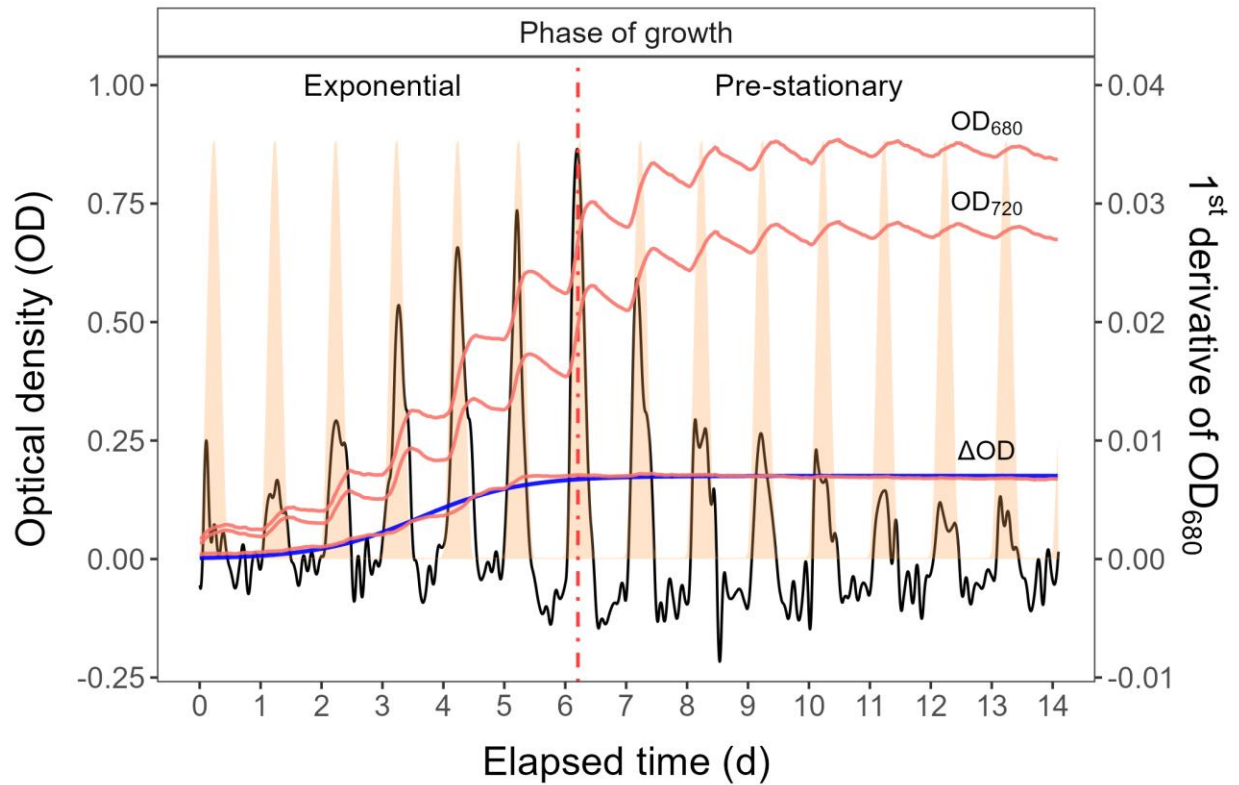
181   growth phases (Fig. 1).

182

Fig. 1. Example of a growth curve (tracked as OD_{720}, OD_{680}, or ΔOD; red solid lines, left y-axis) of PE-rich culture

184   of *Synechococcus* sp. (048) vs. elapsed time (d, x-axis). 1st derivative of OD_{680} taken over 1 h increments (black

185   solid line, right y-axis); solid blue line shows logistic fits of chlorophyll proxy $OD_{680} - OD_{720}$ (ΔOD) vs. elapsed

186   time. The vertical red dot dash line represents the time when the culture reached the maximum of the 1st derivative

187   of OD_{680}, or maximum absolute hourly growth (tMaxAHG), taken as the time of transition from exponential to pre-

188   stationary growth phases.

189

Whole-cell absorbance spectra

191   Absorbance measurements on intact cells in suspension were conducted in an integrating

192   cavity upgrade spectrophotometer (CLARiTY 17 UV/Vis/NIR, On-Line Instrument Systems,

193   Inc., Bogart, GA, USA). 8 mL of f/2 medium were added to both the sample and reference

194   observation cavities of the spectrophotometer. After recording a baseline from 375 to 710 nm, 1

195   mL was withdrawn from the sample cavity and replaced with 1 mL of picocyanobacteria cell

196   suspension. The pathlength corrected absorbance per cm was performed by determining the

197   Jávorfi coefficients (Jávorfi et al. 2006) as described in the equipment manual.

198

Photosynthetically Usable Radiation (PUR)

200   Using whole-cell absorbance spectra of *Synechococcus* sp. cultures (Fig. 2, we estimated

201   Photosynthetically Usable Radiation (PUR; $\mu E = \mu$mol photons m^{-2}s^{-1}) according to (Morel

202   1978). We normalized the obtained whole-cell Absorbances (A) and the Emission spectra of the

203   white LED lamps (Em) from 400 nm to 700 nm to a reference wavelength of 440 nm. PUR is

204   then the ratio of the sum of Absorbance Normalized to 440 nm (NormA$_{440}$) multiplied by the

205   sum of Emission spectra Normalized to 440 nm (NormEm$_{440}$) to the sum of the Emission spectra

206   Normalized to 440 nm (NormEm$_{440}$), multiplied by the PAR (Eq. (1)).

207     $$PUR\ (\mu E) = \frac{\sum(NormA_{440}\ \times\ NormEm_{440})}{\sum(NormEm_{440})}\ \times\ PAR\ (\mu E) \qquad (1)$$
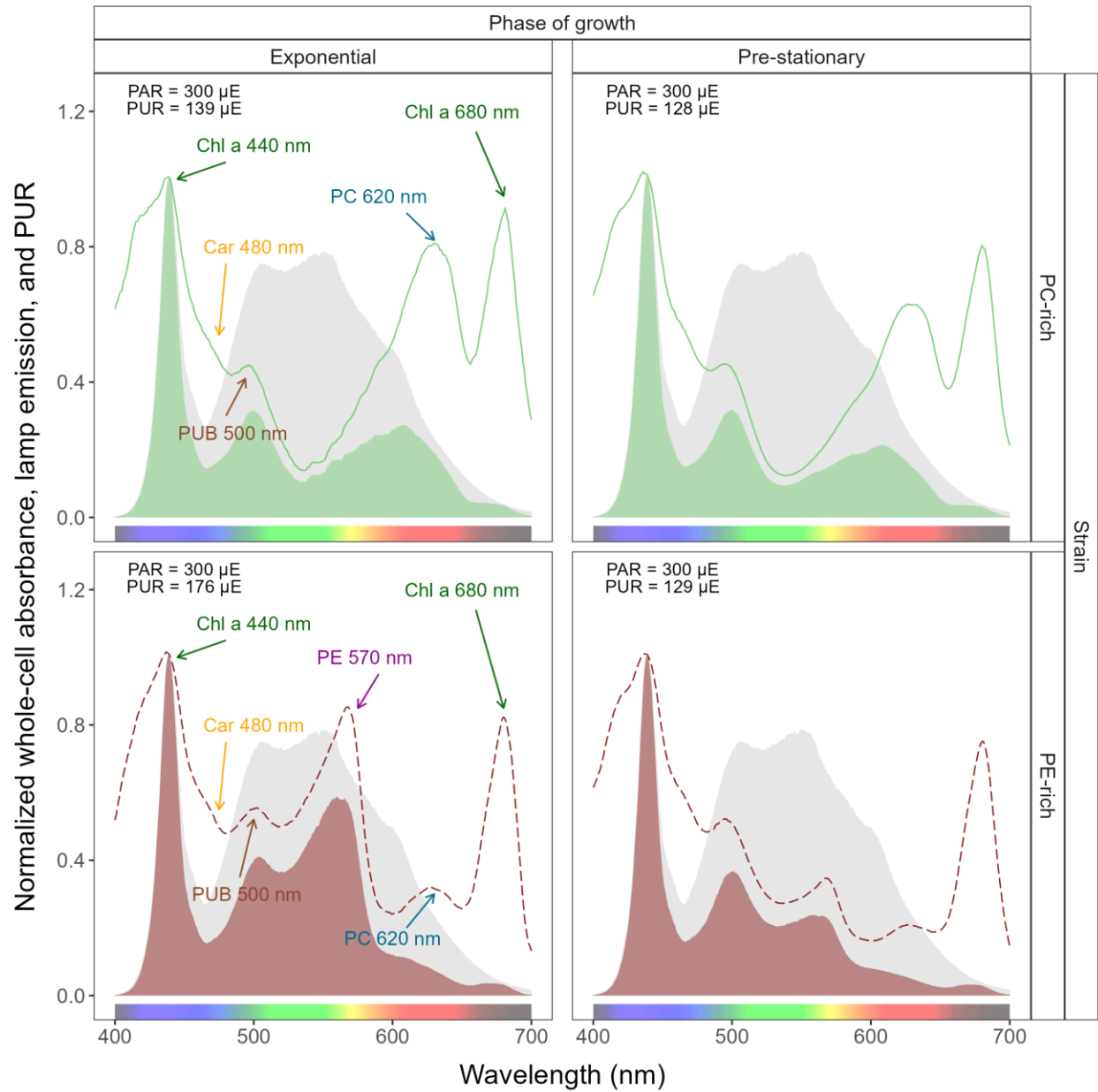
208

Fig. 2. Whole-cell absorbance spectra of PC-rich (solid green lines) or PE-rich (dashed red lines) cultures of

Synechococcus sp. Representative absorbance spectra, normalized to 440 nm (NormA$_{440}$), were measured from the

exponential or pre-stationary phases of growth, together with emission spectra of the white LED lamp used for PAR,

normalized to emission at 440 nm (NormEm$_{440}$, light gray area), in this example PAR was 300 µmol photons m^{-2}s^{-1}.

Estimated Photosynthetically Usable Radiation (PUR) is shown as a darker green area for the PC-rich strain and a

darker red area for the PE-rich strain, with PUR given for each culture (µE = µmol photons m^{-2}s^{-1}). Peaks

216 characteristic of known pigments are labeled; Chl *a*, chlorophyll *a*; PC, phycocyanin; PE, phycoerythrin; PUB,

217 phycourobilin; Car, carotenoids.

218

Cumulative diel PAR and PUR

220   Based on the length and shape of the photoperiod (sinuisoidal wave for photoperiods of 8,

221 12, 16 h; square for photoperiod of 24 h) and the peak PAR ($\mu E = \mu$mol photons m^{-2}s^{-1}), we

222 estimated the value of the cumulative diel PAR (μmol photons m^{-2}d^{-1}). For sinuisoidal

223 photoperiods we used Eq. (2); for the continuous 24 h photoperiod we used Eq. (3). Cumulative

224 diel PUR was estimated similarly after estimation of peak PUR from peak PAR.

225
$$Cumulative\ diel\ PAR\ (\mu mol\ photons\ m^{-2}\ d^{-1}) = \frac{PAR\ (\mu E) \times 60\ (s\ min^{-1}) \times 60\ (min\ h^{-1}) \times photoperiod\ (h\ d^{-1})}{2} \quad (2)$$

226
$$Cumulative\ diel\ PAR\ (\mu mol\ photons\ m^{-2}\ d^{-1}) = PAR\ (\mu E) \times 60\ (s\ min^{-1}) \times 60\ (min\ h^{-1}) \times photoperiod\ (h\ d^{-1}) \quad (3)$$

227

Pigment content

229   Chlorophyll *a* (Chl *a*) (μg mL^{-1}) was measured using Trilogy Laboratory Fluorometer

230 (Turner Designs, Inc., CA, USA) equipped with Chlorophyll In-Vivo Module, previously

231 calibrated using 20 mL ampoules with known Chl *a* concentrations in 3:2 90% acetone:DMSO

232 solution. Quantitative analysis of Chl *a* was obtained after adding 50 μL of culture and 2 mL of a

233 90% acetone:DMSO solution in a 3:2 ratio.

234   We also estimated the pigment content (μg mL^{-1}): chlorophyll *a* (Chl *a*), carotenoids (Car),

235 phycoerythrin (PE), phycocyanin (PC), and allophycocyanin (APC) in *Synechococcus* sp.

236 cultures over time using previously determined linear correlations between pigment content

237 obtained by extraction (Strickland and Parsons 1972; Bennett and Bogorad 1973) and absorbance

238 values of individual pigment peaks (Car; 480, PE; 565, PC; 620, APC; 650, and Chl *a*; 665 nm)

239 obtained from the whole-cell absorbance spectra using integrating cavity upgrade

240 spectrophotometer (CLARiTY 17 UV/Vis/NIR, On-Line Instrument Systems, Inc., Bogart, GA,

241 USA) (Tab. S1 in Supporting Information). The sum of phycobiliproteins (PE, PC, APC protein)

242 to Chl *a* ratio (µg:µg) for individual strains was also calculated.

243

PSII effective absorption cross section of PSII and electron flux

245   We harvested 2 mL of cultures for photophysiological characterizations repeatedly across

246 the growth trajectories. We used Fast Repetition Rate fluorometry (Kolber et al. 1998) (FRRf,

247 Solisense, USA), with a lab built temperature control jacket (22°C), to apply series of flashlets to

248 drive saturation induction/relaxation trajectories, fit using the onboard Solisense LIFT software

249 (Falkowski and Kolber 1993; Kolber et al. 1998). From the model fits we took the initial

250 fluorescence before induction (F_O, F_O', or F_S, depending upon the level of actinic light and step

251 in the light response curve); the maximum fluorescence (F_M or F_M') once Photosystem II (PSII)

252 was driven to closure; and the effective absorption cross section for PSII photochemistry (σ_{PSII} or

253 σ_{PSII}'; nm^2 quanta^{-1}) (Tortell and Suggett 2021). We used a double tap protocol (Xu et al. 2017),

254 where FRRf induction/relaxation trajectories were collected during a rapid light curve sequence

255 increasing in steps of 10 s at 0, 20, 40, 80, 160, and 320 µmol photons m^{-2}s^{-1} PAR, delivered

256 from LED emitters centred at 445, preferentially exciting chlorophyll, or 590 nm, preferentially

257 exciting phycobiliproteins. Flash Power for 445 nm excitation was 60000 µmol photons m^{-2}s^{-1}

258 PAR, while for 590 nm excitation power was 14000 µmol photons m^{-2}s^{-1}, calibrated using a

259 quantum sensor (LI-250, LI-COR, Inc.). We applied 1 s darkness between sequential light steps,

260   to allow re-opening of PSII. FRRf excitation flashlets were applied at the same wavebands, 445

261   or 590 nm, as the actinic light steps.

262   We calculated (Eq. (4)) an uncalibrated fluorescence based estimator for volumetric

263   electron transport, JV_{PSII}, ($k \times e^- \, L^{-1} \, s^{-1}$) under both 445 and 590 nm excitation bands

264   (Oxborough et al. 2012; Boatman et al. 2019; Tortell and Suggett 2021).

$$265 \qquad JV_{PSII} = \frac{\sigma_{PSII}{}' \times qP \times I \times F_O}{\sigma_{PSII}} \qquad (4)$$

266   where σ_{PSII}' is effective absorption cross section for PSII photochemistry under the relevant

267   actinic PAR step ($nm^2 \, quanta^{-1}$); qP is an estimate of the fraction of PSII open for

268   photochemistry estimated according to Oxborough and Baker (1997); I is the applied PAR (µmol

269   photons $m^{-2}s^{-1}$); F_O is the minimum fluorescence from a given sample and excitation bandwidth

270   (relative fluorescence) and σ_{PSII} is the maximum effective absorption cross section for PSII

271   photochemistry from a given sample and excitation bandwidth ($nm^2 \, quanta^{-1}$). We compared

272   several other algorithms for JV_{PSII} (Tortell and Suggett 2021) and found similar results.

273   We calibrated the JV_{PSII} estimator to absolute rates of electron transport (Eq. (5)) using

274   parallel measures of oxygen evolution (µmol $O_2 \, L^{-1} \, s^{-1}$), captured simultaneously with the FRRf

275   measures, below light saturation of electron transport, using a FireSting robust oxygen probe

276   (PyroScience, Germany) inserted in the cuvette for select Rapid Light Curve (RLC) runs (Fig. 3).

277   For the blue LED (Ex_{445nm}) excitation we used a calibration slope of 108832, while for orange

278   LED (Ex_{590nm}) excitation we used a calibration slope of 254327

$$279 \qquad JV_{PSII}(e^- \, L^{-1} \, s^{-1}) = \frac{Uncalibrated \; JV_{PSII}(e^- \, L^{-1} \, s^{-1})}{Calibration \; slope} \qquad (5)$$
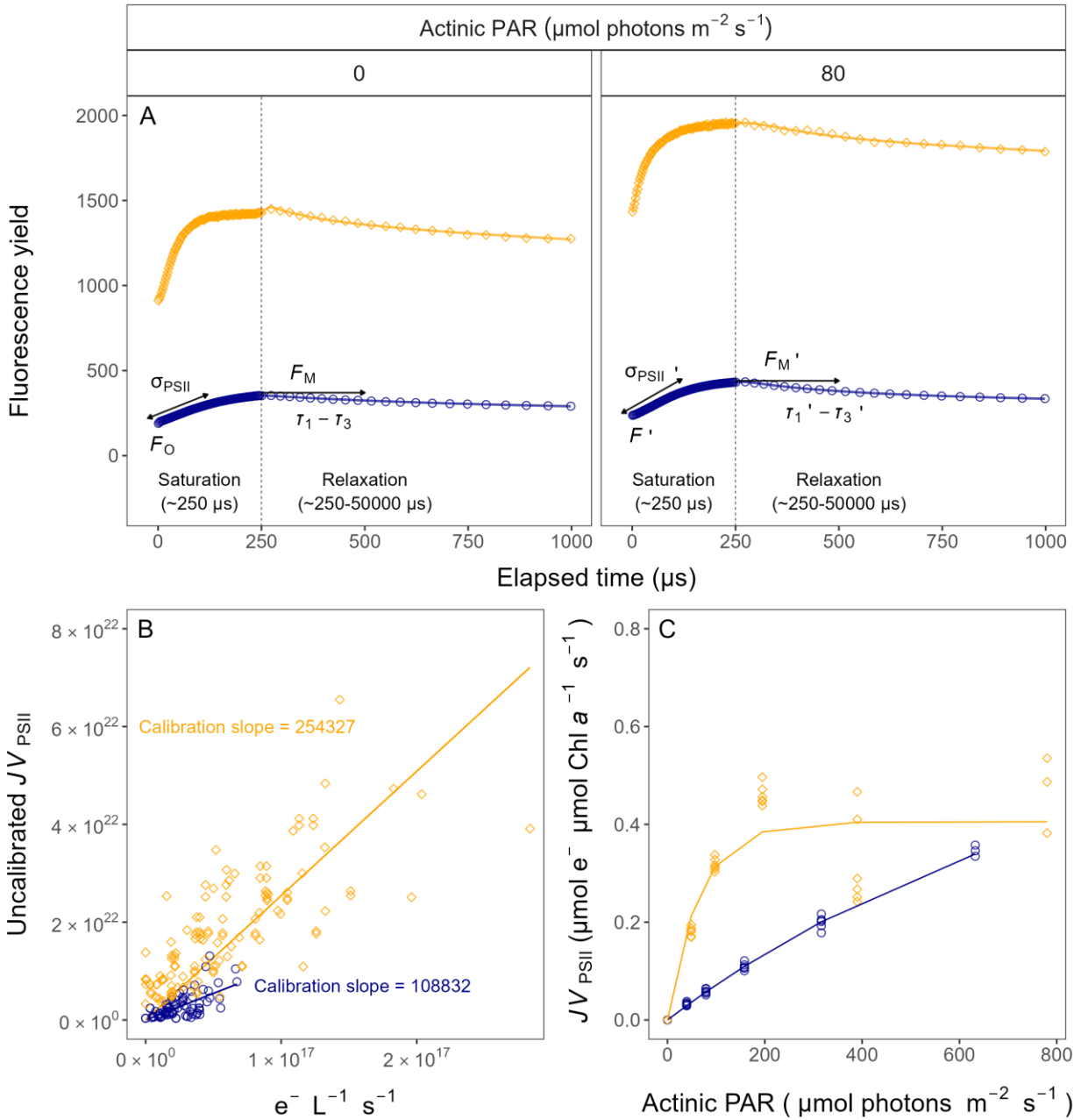
280

281

Fig. 3. Single turnover (ST) fluorescence induction by Fast Repetition Rate fluorometry (FRRf). (**A**) Examples of fluorescence yield vs. elapsed time (μs) for PE-rich culture of *Synechococcus* sp. (048) in the dark (dark-relaxed; 0 μmol photons m^{-2}s^{-1}) and under actinic PAR (in this example 80 μmol photons m^{-2}s^{-1}) using blue LED (Ex$_{445nm}$; open blue circles) or orange (Ex$_{590nm}$; open orange diamonds) excitation. The ST technique delivers a series of flashlets for non-intrusive, repeated monitoring of chlorophyll fluorescence parameters (including F_O, F', F_M, F_M', τ_1-τ_3, τ_1'-τ_3', σ_{PSII}, and σ_{PSII}'). (**B**) Linear regressions of uncalibrated PSII electron flux (JV_{PSII}) vs. e$^-$ L^{-1} s^{-1} derived

15

288   from simultaneously measured oxygen evolution Light Response Curves (LRC) under blue LED (Ex$_{445nm}$; open blue

289   circles) or orange (Ex$_{590nm}$; open orange diamonds) excitation. (**C**) Rapid Light Curve (RLC), fit with a three

290   parameter model (Harrison and Platt 1986), for PSII electron flux (JV_{PSII}; µmol e$^-$ µmol Chl a^{-1} s^{-1}) vs. actinic PAR

291   measured under blue LED (Ex$_{445nm}$; open blue circles) or orange (Ex$_{590nm}$; open orange diamonds) excitation.

292

Statistical analysis

294   We used R version 4.3.0 (R Core Team 2023) running under RStudio (Posit team 2022).

295   We performed three-way factorial ANOVA (*aov()* function; R Base package) to determine

296   whether peak PAR, photoperiod, strain, and their interactions, significantly influence the

297   chlorophyll-specific exponential growth rate (µ; d^{-1}), estimated from logistic fits (*nlsLM()*

298   function; Elzhov et al. (2023)) of chlorophyll proxy $OD_{680} - OD_{720}$ vs. cumulative diel PUR

299   (Table S2). We also used the *nlsLM()* function to fit a three parameter light response model

300   (Harrison and Platt 1986) of growth rates (α, initial slope of curve; *β*, reflecting the

301   photoinhibition process; P_{max}, the maximum rate of growth curve).

302   To examine statistical differences between fits of light responses, we performed one-way

303   ANOVA (*aov()* function) of the three parameter model (Harrison and Platt 1986) fit to pooled

304   data for each taxa, compared to separate fits for each different photoperiod (8, 12, 16, or 24); or

305   to separate fits for each different peak PAR (30, 90, 180, 300, 600 together with 900). These

306   comparisons were run for chlorophyll-specific exponential growth rate vs. cumulative diel PUR

307   (Table S3, S4); vs. cumulative diel PAR (Table S5, S6) or vs. PSII electron flux (JV_{PSII}; µmol e$^-$

308   µmol Chl a^{-1} d^{-1}; Table S7, S8). One-way ANOVA was also used to examine statistical

309   differences between single phase exponential decay fits (*SSasymp()* function; Serway et al.

310   (2004)) of pooled data across different strains for a given phase of growth and across different

311   phase of growth for a given strain for PUR/PAR ratio (Table S9); Phycobiliprotein to Chl a ratio

312 (Table S10); or effective absorption cross section of PSII (σ_{PSII}'; nm^2 quanta^{-1}) measured under

313 diel peak PAR growth light under Ex$_{590nm}$ (orange) excitation in relation to the cumulative diel

314 PAR (μmol photons m^{-2}d^{-1}) (Table S11).

315 We used *t*-tests (*t.test( )* function; R Base package) of linear fits (*lm( )* function) to compare

316 pooled data across different strains for a given phase of growth, and across different phases of

317 growth, for a given strain, for effective absorption cross section of PSII (σ_{PSII}'; nm^2 quanta^{-1})

318 measured under diel peak PAR growth light under Ex$_{445nm}$ (blue) excitation vs. the cumulative

319 diel PAR (μmol photons m^{-2}d^{-1}; Table S12); or vs. the Phycobiliprotein to Chl *a* ratio (Table

320 S13). The same *t*-test analyses were performed for effective absorption cross section of PSII

321 (σ_{PSII}' or σ_{PSII}; nm^2 quanta^{-1}) measured under Ex$_{590nm}$ (orange) excitation vs. the Phycobiliprotein

322 to Chl *a* ratio (Table S14, S15).

323 Statistical differences for all analyses were determined at significance level $\alpha = 0.05$. The

324 manuscript was prepared as a Rmarkdown document (Handel 2020) with figures plotted using

325 ggplot2 (Wickham 2016) and patchwork (Pedersen 2024) packages. All metadata, data and code

326 is available on GitHub (https://github.com/FundyPhytoPhys/BalticPhotoperiod).

327

Results

Chlorophyll-specific exponential growth rate

330 We used logistic curve fits (Fig. S3B) to determine chlorophyll-specific exponential

331 growth rates (μ; d^{-1}), for two PhycoCyanin(PC)-rich cultures (056, 077) and two

332 PhycoErythrin(PE)-rich cultures (048, 127) of *Synechococcus* sp. grown at 30, 90, 180, 300, 600,

333 or 900 peak PAR μmol photons m^{-2}s^{-1} (μE); and photoperiods of 8, 12, 16, or 24 h. Three-way

334 factorial ANOVA showed that peak PAR, photoperiod, strain, and their interactions,

17

335   significantly affected μ (ANOVA, $p < 0.05$ for all; Table S2). All tested strains, except PE-

336   rich_048, grew even under peak PAR 900 µmol photons $m^{-2}s^{-1}$ and 24 h photoperiod. The

337   highest growth rate was recorded for *Synechococcus* sp. PE-rich_127 (μ = 4.5 d^{-1}; 3.7 h doubling

338   time) and PC-rich_056 (μ = 3.4 d^{-1}; 4.9 h doubling time) at 180 µmol photons $m^{-2}s^{-1}$ peak PAR

339   and photoperiod of 24 h.

340   The GAM model in Fig. 4 summarizes the growth responses of the PC-rich and PE-rich

341   picocyanobacteria to peak PAR and photoperiod. PC-rich_056 *Synechococcus* sp. showed

342   highest growth rates under a photoperiod of 24 h, across a wide range of peak PAR indicated by

343   the contour line labeled 1.45 d^{-1}, representing the 90th percentile of achieved growth rates for the

344   strain. On the other hand, the other tested PC-rich strain (077) showed highest growth rates in the

345   range of photoperiod 16-24 h and peak PAR between $300 - 700$ µmol photons $m^{-2}s^{-1}$, indicated

346   by the 1.81 d^{-1} contour line again representing the 90th percentile of maximum achieved growth

347   rates for the strain. For both PC-rich strains, growth was slowest under 30 µmol photons $m^{-2}s^{-1}$

348   and a photoperiod of 8 h.

349   Both PE-rich strains achieved fastest growth rates above peak PAR of ~300 µmol photons

350   $m^{-2}s^{-1}$, under the longest photoperiod of 24 h, indicated by the 1.97 d^{-1} for PE-rich_048, and

351   2.34 d^{-1} for PE-rich_127, contour lines. For the PE-rich strains growth decreased with decreasing

352   photoperiod and decreasing peak PAR. Moreover, PE-rich strains showed photoinhibition of

353   growth at peak PAR of 900 µmol photons $m^{-2}s^{-1}$ and photoperiods of 16- 24 h. The growth rate

354   contours for PC-rich and PE-rich *Synechococcus* sp. did not generally follow isoclines of

355   cumulative diel photon dose (µmol photons $m^{-2}d^{-1}$, dashed lines), showing that photoperiod, and

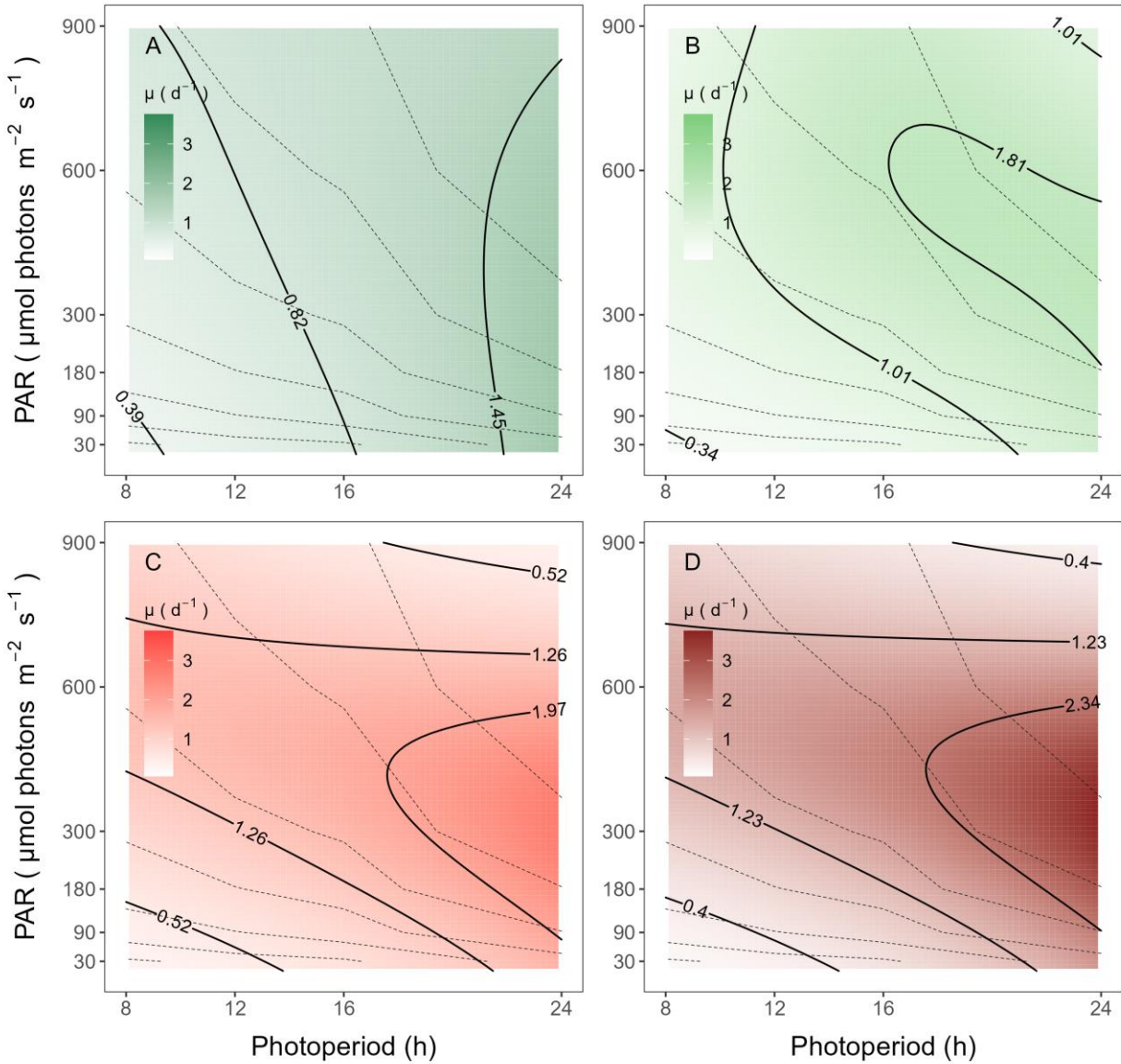356   peak PAR influenced growth rates beyond cumulative diel photon dose.

Fig. 4. A contour plot of a Generalized Additive Model (GAM) of chlorophyll-specific growth rates (d^{-1}) for two PC-rich cultures: (**A**) 056, (**B**) 077 and two PE-rich cultures: (**C**) 048, (**D**) 127 of *Synechococcus* sp. grown at 30, 90, 180, 300, 600, or 900 peak PAR µmol photons m^{-2}s^{-1}; and photoperiods of 8, 12, 16, or 24 h. Legends show colour gradients of growth rate (μ; d^{-1}) from no growth (white) to 3.0 d^{-1} (dark green for PC-rich_056, light green for PC-rich_077, light red for PE-rich_048 or dark red for PE-rich_127 strains). Labeled contour lines indicate the 90%, 50%, and 10% quantiles for achieved growth rate. Dotted lines show isoclines of cumulative diel photon dose (µmol photons m^{-2}d^{-1}).

366   A three parameter light response model fit (Harrison and Platt 1986) of chlorophyll-

367   specific exponential growth rates vs. cumulative diel PUR dose for two PC-rich and two PE-rich

368   cultures of *Synechococcus* sp. showed significant differences between model fits of the pooled

369   data vs. fits for all tested photoperiods (8, 12, 16, or 24 h; ANOVA, $p < 0.05$; Fig. 5A, Table S3).

370   The alpha parameters of the initial rise of growth rate (α) vs. cumulative diel PUR, estimated

371   from data pooled for each photoperiod increased with increasing photoperiod for all strains. The

372   highest increase (>2-fold) of α with increasing photoperiod was recorded for PC-rich_056 (Fig.

373   5B). Strains also showed distinct growth rate responses to cumulative diel PUR, depending upon

374   peak PAR (Fig. S4A, Table S4), that differ from a single light response model fit to the pooled

375   data across all peak PAR from a strain. Exceptions were observed in the strains PC-rich_077 and

376   PE-rich_048 with the peak PAR of 600 or 900 µmol photons $m^{-2}s^{-1}$, which were not

377   significantly different from the pooled data model. A caveat to these findings is that cumulative

378   diel photon dose is a product of photoperiod and PAR, so the highest levels of cumulative PUR

379   dose are only achieved under the 600 or 900 µmol photons $m^{-2}s^{-1}$. The alpha parameters of the

380   initial rise of growth rate (α) vs. cumulative diel PUR, estimated from data pooled for each peak

381   PAR decreased across peak PAR for all tested strains (Fig. S4B).

382   Growth rate saturated under increasing cumulative diel PUR for all strains, however, the

383   achieved estimates of μ_{max} varied depending upon photoperiod and peak diel PAR. Growth rates

384   vs. cumulative diel PAR relationships, estimated for exponential phase cultures, followed similar

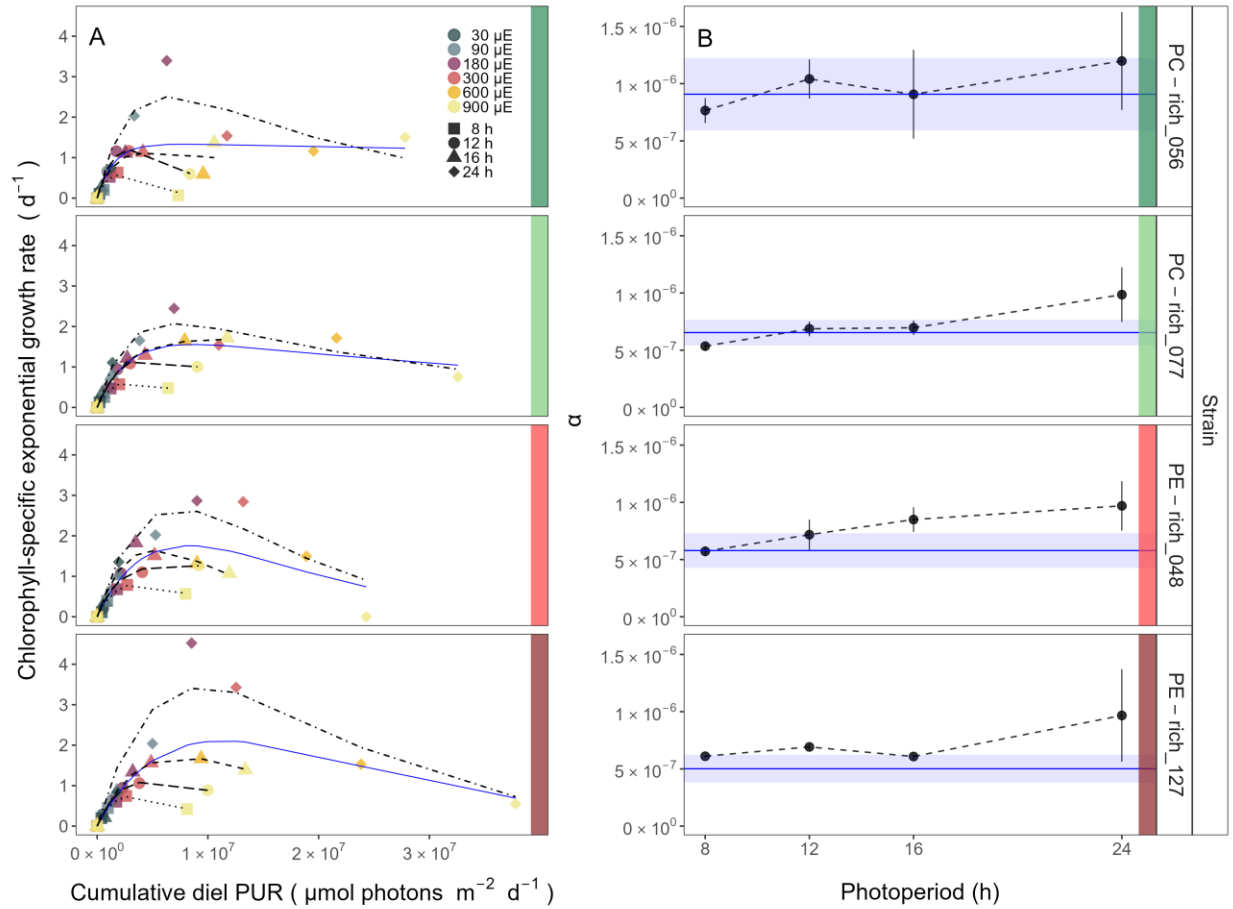385   patterns (Fig. S5, Fig. S6 and Table S5, S6 in Supporting Information).

386

Fig. 5. (**A**) Chlorophyll-specific exponential growth rates (d^{-1}) vs. cumulative diel Photosynthetically Usable

Radiation (PUR, µmol photons $m^{-2}d^{-1}$). Growth rates ($\pm$ SE falling within symbols) were estimated from logistic fits

of chlorophyll proxy $OD_{680} - OD_{720}$ (ΔOD) vs. elapsed time (Fig. 1, Fig. S3B), for two PC-rich cultures (056; dark

green, 077; light green) and two PE-rich cultures (048; light red, 127; dark red) of *Synechococcus* sp. grown at 30

(dark gray), 90 (light gray), 180 (purple), 300 (red), 600 (orange), or 900 (yellow) peak PAR µmol photons $m^{-2}s^{-1}$

(μE); and photoperiods of 8 (square), 12 (circle), 16 (triangle), or 24 (diamond) h. Solid blue line shows a fit of the

pooled growth rates through photoperiods for each strain, with a three parameter model (Harrison and Platt 1986).

We also fit the same model separately for 8 (dotted line), 12 (long dash line), 16 (dashed line), or 24 (two dash line)

h photoperiods, since for all strains they were each significantly different (ANOVA, $p < 0.05$) from the fit of pooled

data. (**B**) Alpha parameters of the initial rise of growth rate (α) vs. cumulative diel Photosynthetically Usable

Radiation (PUR), estimated from data pooled for each photoperiod (points ($\pm$ SE) connected by dashed lines), and

estimated for all data across photoperiods (solid blue horizontal line $\pm$ SE), for each strain.

21

399

PUR/PAR ratio vs. cumulative diel PAR

The PUR/PAR ratio is an index of the efficacy of light capture for a culture under a given growth condition; showing the fraction of PAR that can be captured by the absorbance of the cells (Fig. 6). For the two PC-rich and, particularly, for the two PE-rich cultures of *Synechococcus* sp. PUR/PAR decayed exponentially to a plateau, with increasing cumulative diel PAR, when pooling PUR/PAR data across different combinations of photoperiod and peak PAR. Although all strains followed a similar trend, the single phase exponential decay model fit parameters varied significantly among strains, during their exponential phase of growth (ANOVA, $p < 0.05$), except the model fits from PE-rich_048 and PE-rich_127 (ANOVA, $p > 0.05$; Table S9). Moreover, the PUR/PAR ratio was higher in the PE-rich strains under low cumulative diel photon dose during their exponential phase of growth (y_0 greater or equal to 0.9), but decayed towards a plateau close to the PC-rich strains as cumulative diel photon dose increases ($y_f = 0.5$). On the other hand, the single phase exponential decay model fits did not differ significantly among strains, during their pre-stationary phase of growth (ANOVA, $p > 0.05$; Table S9). During this phase, response of PUR/PAR ratio to increasing cumulative diel PAR exhibits damping, maintaining a consistent trend across all strains within the y_f range of 0.4 to 0.5, with the exception of the PE-rich_048 strain. We also find that model fits from different phases of growth differed within a given strain, with the exception of PC-rich_056 (ANOVA; $p < 0.05$, Table S9). A similar decay trend was observed for Phycobiliprotein to Chl *a* ratio ($\mu g:\mu g$) across cumulative diel PAR (Fig. S7).

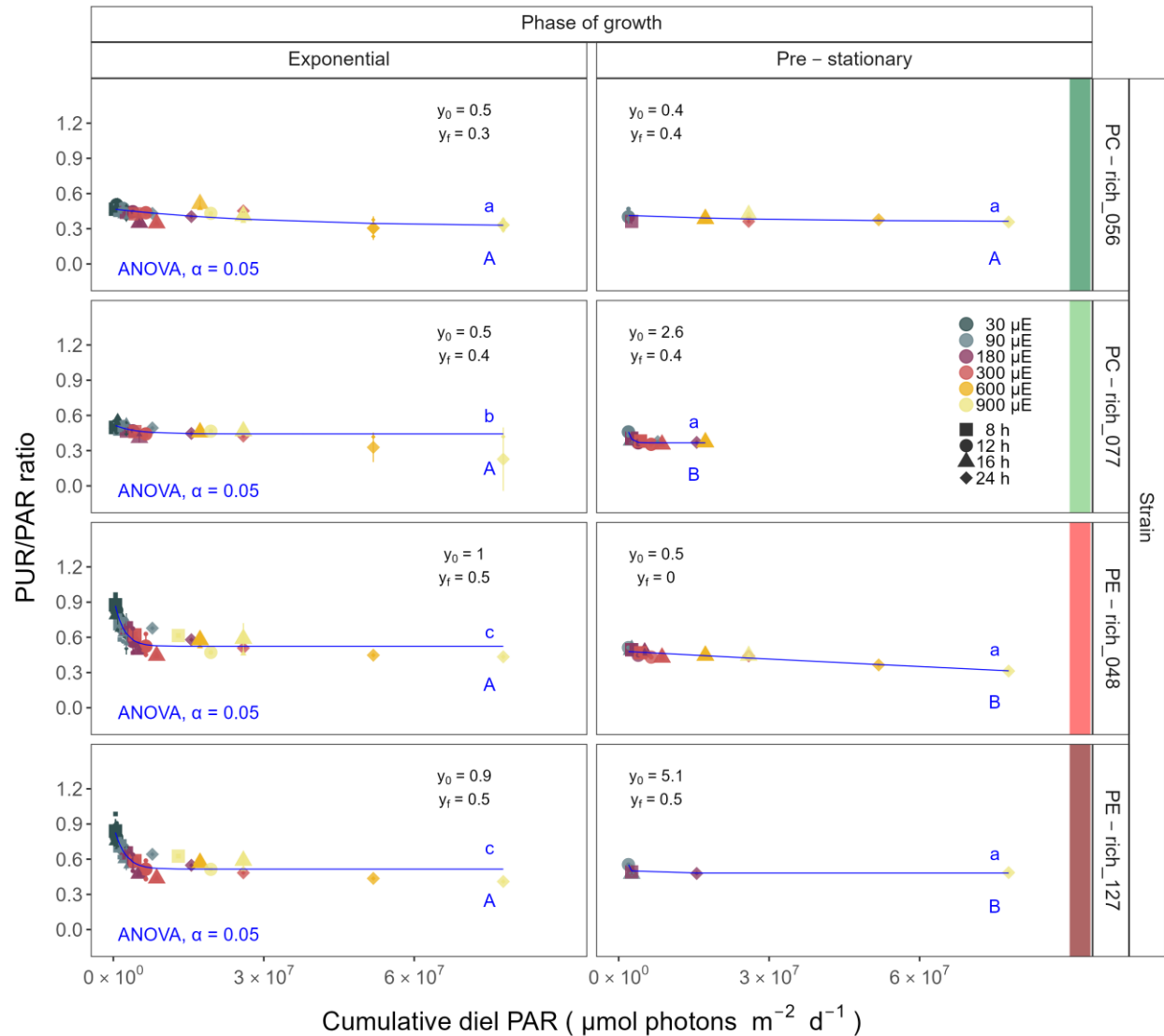**Fig. 6.** Changes in PUR/PAR ratio vs. cumulative diel PAR (µmol photons $m^{-2}d^{-1}$). PUR/PAR ratio was estimated for two PC-rich cultures (056; dark green, 077; light green) and two PE-rich cultures (048; light red, 127; dark red) of *Synechococcus* sp. grown at 30 (dark gray), 90 (light gray), 180 (purple), 300 (red), 600 (orange), or 900 (yellow) peak PAR µmol photons $m^{-2}s^{-1}$ (µE); and photoperiods of 8 (square), 12 (circle), 16 (triangle), or 24 (diamond) h. Figure presents data (smaller symbols) and means (bigger symbols) from exponential or pre-stationary phase of growth. Blue solid line shows single phase exponential decay fit for data from each strain and growth phase, with fit parameters presented. Different lowercase letters indicate statistically significant differences between the fit models for different strains within a given phase of growth. Different uppercase letters indicate statistically significant differences between the fit models for different phases of growth within a given strain (ANOVA; $p < 0.05$).

23

430

Effective absorption cross section of PSII of picocyanobacteria

The effective absorption cross section of PSII (σ_{PSII}', nm^2 quanta^{-1}), was estimated using FRRf induction curves using Ex$_{590nm}$ (orange) excitation, for two PC-rich (056, 077) and two PE-rich (048, 127) cultures of *Synechococcus* sp. grown at 30, 90, 180, 300, 600, or 900 peak PAR µmol photons m^{-2}s^{-1} (µE); and photoperiods of 8, 12, 16, or 24 h (Fig. 7). The σ_{PSII}' measured under diel peak PAR growth light under Ex$_{445nm}$ (blue) excitation vs. cumulative diel photon dose is shown in Supporting Information (Fig. S8, Table S12).

All strains showed consistent patterns of sharp, exponential decay of effective absorption cross section for PSII photochemistry vs. cumulative diel photon doses, across different combinations of photoperiod and peak PAR (Fig. 7A). Although all strains showed this response pattern, the exponential decay fits differed significantly among two PC-rich strains and PE-rich_048 strains during their exponential phase of growth (ANOVA, $p < 0.05$; Table S11). PE-rich strains showed higher σ_{PSII}' under low cumulative diel photon dose (y$_0$ about 0.8 and y$_f$ about 4) than did PC-rich strains. During pre-stationary phase this response dampens in the PC-rich strains but persists in the PE-rich strains (Table S11). σ_{PSII}' for the PE-rich strains during pre-stationary phase of growth still remain higher (y$_f$ between 2.3 – 3.0) than in the PC-rich strains (y$_f$ between 1.4 – 1.7) even as cumulative diel photon dose increases. Model fits from different phases of growth differed within a given strain, with the exception of PE-rich_048 (ANOVA; $p < 0.05$, Table S11).
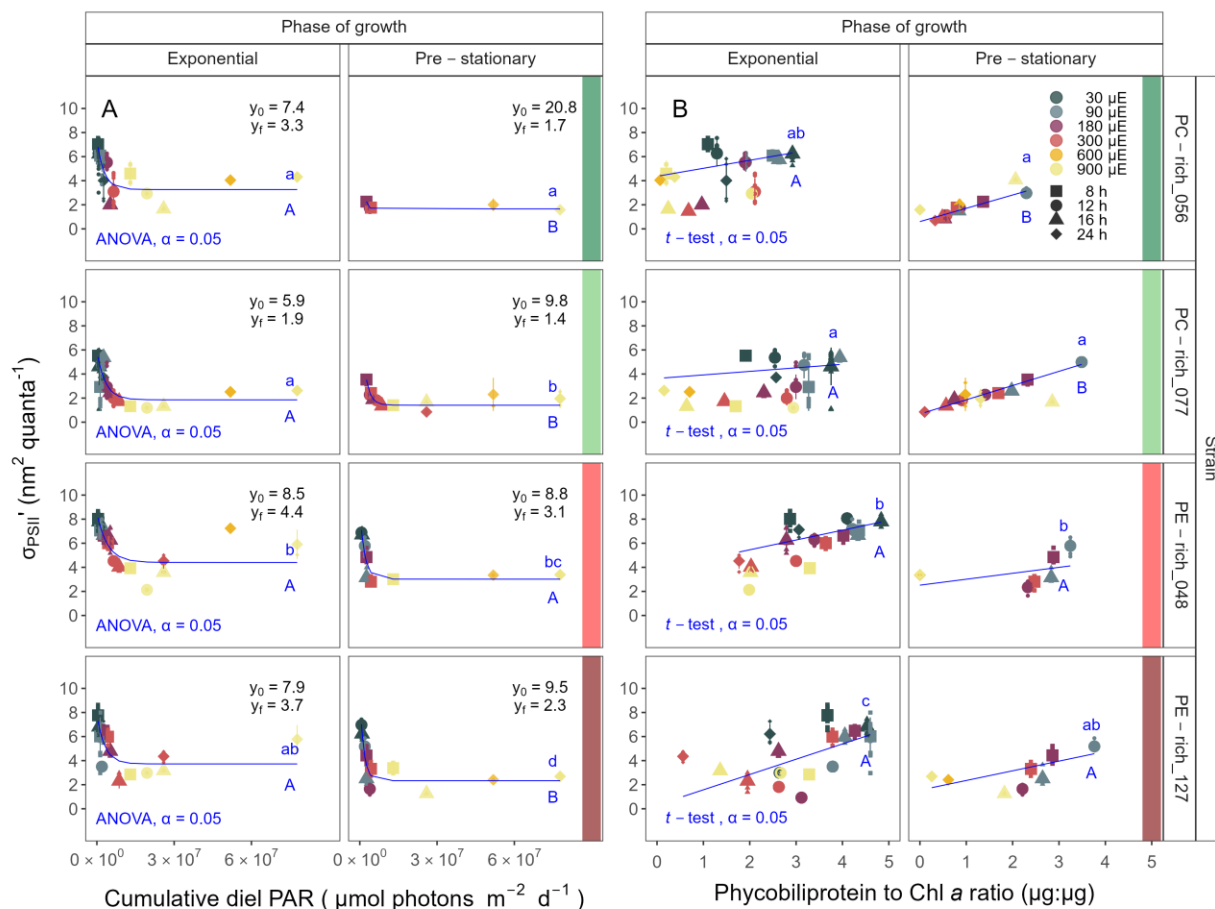
Fig. 7. (A) Effective absorption cross section of PSII (σ_{PSII}'; nm^2 quanta^{-1}) measured under diel peak PAR growth light vs. cumulative diel PAR (μmol photons m^{-2}d^{-1}); blue solid line shows single phase exponential decay fit for data from each strain and growth phase. **(B)** Changes of σ_{PSII}' measured under diel peak PAR growth light vs. the ratio of sum of μg phycobilins (PE, PC, APC protein, Phycobiliprotein) to μg Chl *a*; blue solid line shows linear model fit for data from each strain and growth phase. σ_{PSII}' was estimated using FRRf induction curves with excitation of phycobilisomes (Ex$_{590nm}$, orange), for two PC-rich cultures (056; dark green, 077; light green) and two PE-rich cultures (048; light red, 127; dark red) of *Synechococcus* sp. grown at 30 (dark gray), 90 (light gray), 180 (purple), 300 (red), 600 (orange), or 900 (yellow) peak PAR μmol photons m^{-2}s^{-1} (μE); and photoperiods of 8 (square), 12 (circle), 16 (triangle), or 24 (diamond) h. Figure presents data (smaller symbols) and means (bigger symbols) from exponential or pre-stationary phase of growth. Different lowercase letters indicate statistically significant differences between the fit models for different strains within a given phase of growth. Different

25

462   uppercase letters indicate statistically significant differences between the fit models for different phases of growth

463   within a given strain ($p < 0.05$).

464

465   Effective absorption cross section of PSII (σ_{PSII}'; nm^2 quanta^{-1}), measured under diel peak

466   PAR growth light with Ex_{590nm} (orange) excitation, varies with Phycobiliprotein to Chl a ratio

467   (Fig. 7B). σ_{PSII}' excited through phycobilisome absorbance at Ex_{590nm} shows positive linear

468   correlations with the Phycobiliprotein to Chl a ratio, although strains in exponential growth show

469   significant scatter around this positive relation, likely related to regulatory control of σ_{PSII}' under

470   different measurement PAR, beyond pigment composition. Under pre-stationary phase the

471   relationship between σ_{PSII}' and Phycobiliprotein to Chl a ratio was more consistent, suggesting

472   increased reliance upon compositional regulation to control light delivery to PSII, as opposed to

473   shorter-term physiological regulation under changing light. The linear fits of σ_{PSII}'

474   vs. Phycobiliprotein to Chl a ratio also vary significantly between PC-rich_077 and two PE-rich

475   strains during their exponential phase of growth. During pre-stationary phase we noted

476   significant differences between two PC-rich strains and PE-rich_048. Moreover, significant

477   differences between the fit models for varying phases of growth were noted for PC-rich strains

478   056 and 077 (t-test; $p < 0.05$, Table S14).

479   Changes in effective absorption cross section of PSII (σ_{PSII}; nm^2 quanta^{-1}) measured in the

480   dark with Ex_{590nm} (orange) excitation vs. Phycobiliprotein to Chl a ratio (Fig. S9A, Table S15)

481   and σ_{PSII}' measured under diel peak PAR growth light under Ex_{445nm} (blue) excitation

482   vs. Phycobiliprotein to Chl a ratio (Fig. S9B and Table S13) are shown in Supporting

483   Information.

484

Growth rates vs. cumulative diel PSII electron flux

Chlorophyll-specific exponential growth rates (d^{-1}), within each strain, show fairly consistent saturating responses to increasing cumulative diel PSII electron flux (JV_{PSII}; µmol e^- µmol Chl a^{-1} d^{-1}) estimated under diel peak PAR growth light, and estimated using FRRf induction curves with excitation of chlorophyll (Ex_{445nm}, blue), although photoperiod (Fig. 8A, Table S7) and peak PAR (Fig. S10, Table S8) retained a secondary influence on achieved growth responses for some growth conditions.

A three parameter model fit of (Harrison and Platt 1986) vs. cumulative diel PSII electron flux (JV_{PSII}; µmol e^- µmol Chl a^{-1} d^{-1}) for two PC-rich and two PE-rich cultures of *Synechococcus* sp. showed no significant differences between fits of the pooled data vs. fits for different photoperiods (8, 12, 16, or 24 h; ANOVA, $p < 0.05$), with exception of 8 and 24 h photoperiod for PC-rich_056 and 8 h photoperiod for PE-rich_127 strains (ANOVA, $p > 0.05$; Table S7).

Alpha parameters of the initial rise of growth rate (α) vs. cumulative diel JV_{PSII}, estimated from data pooled for each photoperiod showed an increase across increasing photoperiods for each strain except for PE-rich_0127. The highest increase (>2-fold) of α from the lowest to the highest photoperiod was recorded for PC-rich_077 (Fig. 8B).
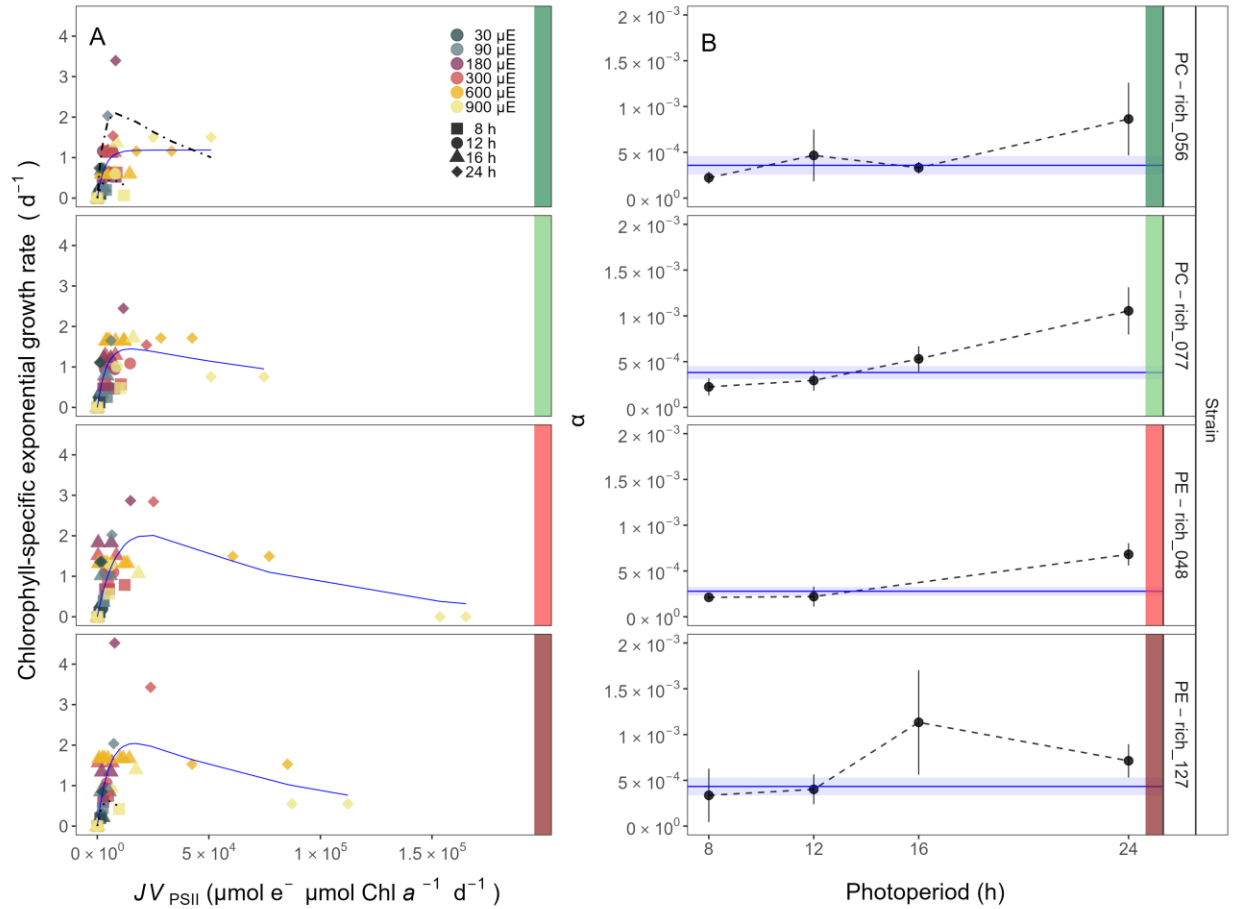
502

Fig. 8. (**A**) Chlorophyll-specific exponential growth rates (d^{-1}) vs. cumulative diel PSII electron flux (JV_{PSII}; μmol e^- μmol Chl a^{-1} d^{-1}) measured under diel peak PAR growth light. Growth rates ($\pm$ SE falling within symbols) were estimated from logistic fits of chlorophyll proxy OD_{680} - OD_{720} (ΔOD) vs. elapsed time (Fig. S3B). JV_{PSII} was estimated using FRRf induction curves with excitation of chlorophyll (Ex_{445nm}, blue), for two PC-rich cultures (056; dark green, 077; light green) and two PE-rich cultures (048; light red, 127; dark red) of *Synechococcus* sp. grown at 30 (dark gray), 90 (light gray), 180 (purple), 300 (red), 600 (orange), or 900 (yellow) peak PAR μmol photons $m^{-2}s^{-1}$ (μE); and photoperiods of 8 (square), 12 (circle), 16 (triangle), or 24 (diamond) h. Solid blue line shows a fit of the pooled growth rates for each strain, with a three parameter model (Harrison and Platt 1986). We also fit the same model separately for 8 (dotted line) and 24 (two dash line) h photoperiods, when they were significantly different (ANOVA, $p < 0.05$) from the fit of pooled data. (**B**) Alpha parameters of the initial rise of growth rate (α) vs. cumulative diel JV_{PSII}, estimated from data pooled for each photoperiod (points ($\pm$ SE) connected by dashed lines), and estimated for all data across photoperiods (horizontal line $\pm$ SE), for each strain.

28

515

Discussion

Photic regimes - implications for picocyanobacteria growth and distribution

Light regimes, including photoperiod, and peak PAR, are major factors affecting the distribution and seasonality of phytoplankters (Erga and Heimdal 1984). Changes in photoperiod trigger acclimation responses, shaping the temporal dynamics and community structure of phytoplankton (Theus et al. 2022; Longobardi et al. 2022). Each tested picocyanobacterial strain showed influences of photoperiod upon the responses of growth rate to cumulative diel PUR (Fig. 5) and PAR (Fig. S5). To our surprise, increasing photoperiod increased the ranges of response to PAR and PUR. Both the PC-rich and the PE-rich strains of *Synechococcus* sp. exhibited their highest initial responses of growth to increasing PUR and PAR (alpha, (Fig. 5B), Fig. S5B), and their fastest growth rates under continuous light (24 h photoperiod), consistent with some other strains (Jacob-Lopes et al. 2009; Klepacz-Smółka et al. 2020). Yet, 24 h photoperiod also exacerbated eventual photoinhibition under excess cumulative diel PUR and PAR. Our temperate strains do not experience direct selective pressures to exploit a continuous 24 photoperiod (Brand and Guillard 1981), so achieving maximum growth under a 24 h photoperiod rather suggests lack of a requirement for a dark period, and lack of requirement for a regular photoperiod. Coastal phytoplankton strains are selected to exploit instantaneous light (Brand and Guillard 1981), of whatever duration, to cope with fluctuating light and nutrients in coastal environments (MacIntyre et al. 2000; Litchman et al. 2009), leading to a pleiotropic capacity for exploiting continuous light. The ability of both PC-rich and PE-rich coastal picocyanobacteria to exploit continuous light means they could, potentially, grow rapidly at higher latitudes, in a future warmer polar summer water.

538   Light level is another key driver of picocyanobacteria productivity (Pick 1991; Six et al.

539 2007; Aguilera et al. 2023). The spatial and temporal distribution of PAR within aquatic

540 ecosystems is influenced by solar angle, water depth, water clarity, and the presence of light-

541 absorbing substances such as dissolved organic matter (Morel 1978, 1988) and phytoplankton

542 cells. PUR then represents the light potentially available for phytoplankton to photosynthesize.

543 PUR is always smaller than PAR (PUR < PAR), and depends on the spectral composition of the

544 PAR, versus the phytoplankton pigment composition, determining cellular spectral absorption

545 (Morel 1978), which changes depending upon growth conditions and the phase of growth.

546   PE-rich and PC-rich *Synechococcus* sp. strains show distinct growth responses to

547 cumulative diel photon dose, depending upon the peak PAR of the applied photoregime (Fig. S4,

548 Fig. S6). Chlorophyll-specific exponential growth rates of the PE-rich and PC-rich

549 *Synechococcus* sp. strains increased with increasing light levels, to a plateau in the range of 180

550 – 300 µmol photons $m^{-2}s^{-1}$. Growth above 600 µmol photons $m^{-2}s^{-1}$ occurred with a growth

551 yield per cumulative diel photon lower than under moderate light, particularly when combined

552 with short 8 h or long 24 h photoperiods. Even though PE-rich *Synechococcus* sp. are more

553 adapted to lower-light conditions deeper in the water column (Stomp et al. 2007), our findings

554 show that PE-rich strains will grow under higher irradiance.

555   The maximum growth rate of *Synechococcus* sp. PE-rich_127 strain under 24 h

556 photoperiod and peak PAR of 180 µmol photons $m^{-2}s^{-1}$ was 4.5 d^{-1} (µ = 0.187 h^{-1}),

557 corresponding to a doubling time of 3.7 h (Fig. 5, Fig. S4); faster than previously reported for

558 marine picocyanobacteria, and indeed faster than for the model freshwater cyanobacteria

559 *Synechococcus* sp. PCC6301 (doubling time of 4.5-5 h under constant illumination and 250 µmol

560 photons $m^{-2}s^{-1}$) (Sakamoto and Bryant 1999), or *Synechocystis* sp. PCC 6803 (doubling time of

561 4.3 h) (van Alphen et al. 2018). The fastest growth rate as yet achieved for any phytoplankter

562 occurs in a genetically modified green algae *Picochlorum celeri*, with a maximum of about 6.8

563 d^{-1} and ~2.5 h doubling time, in bioreactors (Krishnan et al. 2021). The Baltic *Synechococcus* sp.

564 strains, not genetically modified, preferred 24 h photoperiod and moderate peak PAR of 180

565 µmol photons $m^{-2}s^{-1}$, suggesting they could, potentially, thrive in warming polar latitude waters.

566 *Synechococcus* sp. strains indeed already occur across geographical regions (Śliwińska-

567 Wilczewska et al. 2018b) with different photic regimes, including polar regions (reviewed by

568 Velichko et al. (2021)), exceeding latitude 80°S and 80°N. The prolonged daylight hours of polar

569 summers, coupled with nutrient-rich waters, promote growth of genetically diverse

570 *Synechococcus* populations (Vincent et al. 2000), contributing significantly to primary

571 productivity. Gradinger and Lenz (1989) suggested that *Synechococcus*-type picocyanobacteria

572 may serve as indicator organisms for the advection of warm water masses into polar regions,

573 important in the context of monitoring upcoming climate changes.

574   The coastal PC-rich and PE-rich strains of *Synechococcus* showed saturation, and then

575 photoinhibition of growth rates under increasing cumulative diel PUR, although the achieved

576 estimates of μ_{max}, and the onset of photoinhibition of growth, varied depending upon strain,

577 photoperiod and peak PAR (Fig. 4). The tested strains were generally opportunistic in exploiting

578 longer photoperiods to achieve faster µ, although PE-rich strains suffered strong photoinhibition

579 of growth under peak PAR above 600 µmol photons $m^{-2}s^{-1}$ and 24 h photoperiod (Fig. 5, Fig.

580 S4), suggesting the PE-rich strains are better adapted to lower light and deeper parts of the water

581 column. The least favorable growth conditions for both PE-rich and PC-rich strains of

582 *Synechococcus* sp. were under high light (> 600 µmol photons $m^{-2}s^{-1}$) and the shortest

583 photoperiod (8 h), even though the cumulative diel PUR dose was equivalent to conditions where

584   the light intensity was lower and the photoperiod was longer. Thus these Baltic

585   picocyanobacteria are prone to photoinhibition under both the longest, and the shortest,

586   photoperiod regimes, with flatter light responses of growth under intermediate photoperiods.

587   Thus, in regions and periods with a longer photoperiod, both PC-rich and PE-rich *Synechococcus*

588   sp. could become dominant species in surface waters, but could suffer under shorter
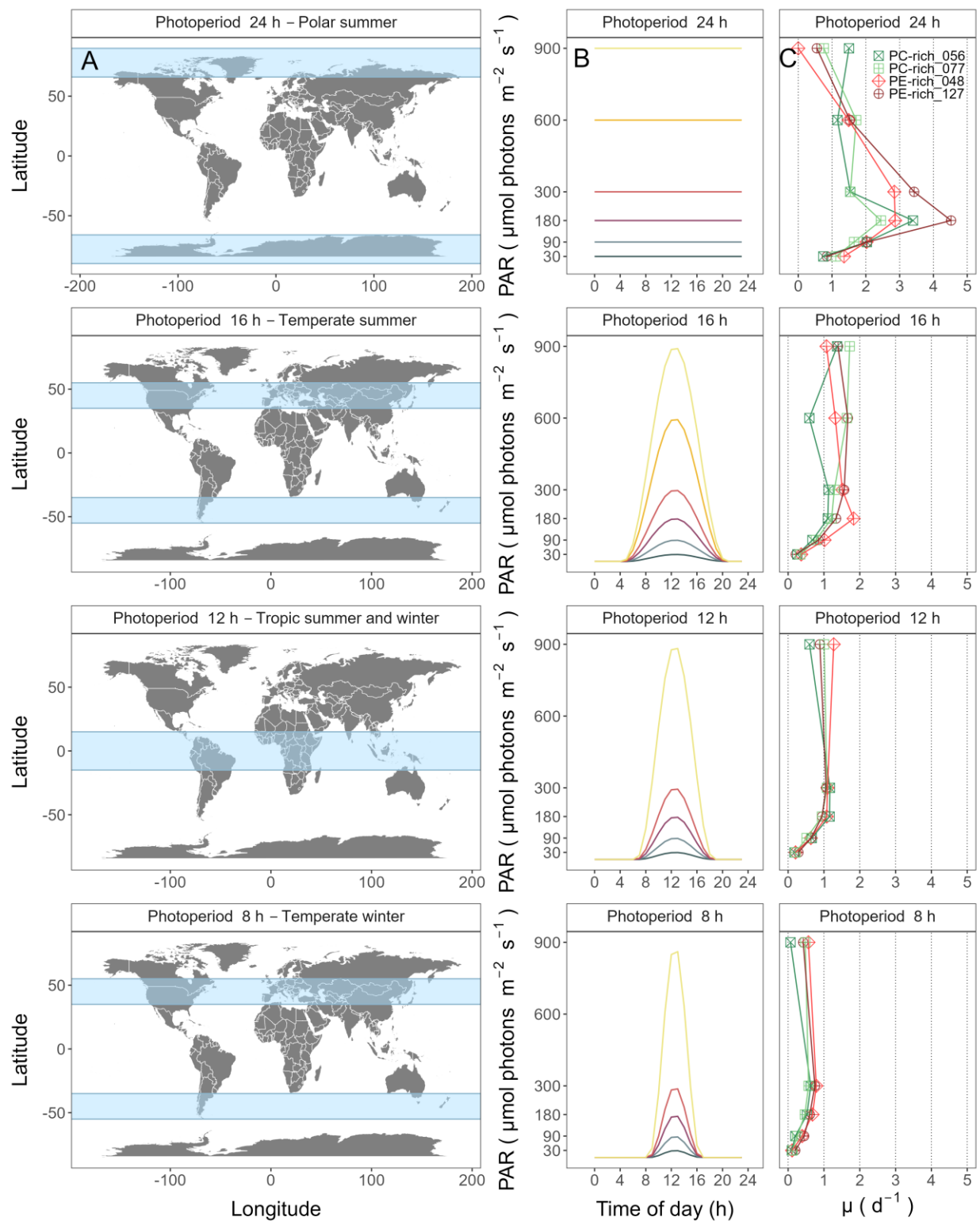
589   photoperiods (Fig. 9).

590

Fig. 9. Latitudinal bands, equivalent summer or winter photoperiods, and picocyanobacterial growth responses. (**A**)

Latitudinal bands corresponding to tested growth photoperiods. (**B**) Tested photoperiod and peak PAR regimes used

593   for growth experiments. (**C**) Chlorophyll specific exponential growth rates (± SE falling within symbols) for two

594   PhycoCyanin(PC)-rich cultures (056; dark green, 077; light green) and two PhycoErythrin(PE)-rich cultures (048;

595   light red, 127; dark red) of *Synechococcus* sp. under tested photoperiod and peak PAR regimes.

596

Photic regimes and growth phase both influence cellular absorbance and light use

599   Under nutrient replete exponential growth the picocyanobacterial strains show consistent

600   patterns of an exponential decline in PUR/PAR ratio versus cumulative diel photon doses, across

601   different combinations of photoperiod and peak PAR. Thus, under nutrient repletion the

602   picocyanobacteria balance pigment composition to match light conditions (Fig. 6). In addition to

603   chlorophyll *a*, picocyanobacteria use phycobilins, including phycocyanin (harvesting red light at

604   620 nm) and phycoerythrin (harvesting yellow light at 570 nm), as accessory pigments to

605   enhance light harvesting efficiency. Picocyanobacteria enhance phycobilin production to

606   compensate for limited irradiance, thereby optimizing their photosynthetic capabilities

607   (Śliwińska-Wilczewska et al. 2018a) and increasing their PUR/PAR.

608   The effective absorption cross section for photochemistry of PSII in the light (σ_{PSII}')

609   comprises the probability of light capture by PSII and the quantum yield for subsequent

610   photochemistry. PC-rich and PE-rich strains of *Synechococcus* again show consistent patterns of

611   an exponential decay to a plateau with increasing cumulative diel PAR doses, for σ_{PSII}' (nm^2

612    $quanta^{-1}$, measured under diel peak PAR growth light under Ex_{590nm} (orange) excitation), without

613   detectable influences of photoperiod, nor of peak PAR (Fig. 7A). σ_{PSII}' excited through

614   chlorophyll absorbance at 445 nm was, in contrast, consistently small across strains and growth

615   conditions (Fig. S8, Fig. S9), since in cyanobacteria the number of chlorophyll serving each PSII

616   is nearly fixed (Xu et al. 2018). σ_{PSII}' excited through phycobilisome absorbance at 590 nm

617   shows, as expected, a positive correlation with Phycobiliprotein:Chl *a*. Growth under low

618   cumulative diel PAR results in an increased Phycobiliprotein:Chl *a*, as the picocyanobacteria

619   allocate protein resources towards phycobiliprotein-mediated light capture (Beale 1994;

620   Stadnichuk et al. 2015; Chakdar and Pabbi 2016). PC-rich and PE-rich strains of *Synechococcus*

621   sp. in exponential growth nonetheless show significant scatter around this pattern, likely related

622   to regulatory control of σ_{PSII}', beyond pigment composition. In pre-stationary phase σ_{PSII}'

623   vs. Phycobiliprotein:Chl *a* was better aligned, suggesting reliance upon fixed compositional

624   regulation of phycobiliprotein content to control light delivery to PSII, as opposed to shorter-

625   term regulation.

626   A phylogeny 16S rRNA gene phylogeny (amplicon average 1385 bp) placed the tested

627   strains in order Synechococcales and family Synechoccaceae, within the cluster 5

628   picocyanobacterial lineage, in sub-cluster 5.2 together with freshwater, brackish and halotolerant

629   strains, separated from marine sub-clusters 5.1 and 5.3 (Fig. 1S). The 16S rRNA of the strains

630   showed ∼100% identity with strains assigned to *Synechococcus* spp. or to *Cyanobium* spp. It is

631   worth emphasizing that light capture and light absorption abilities differed significantly among

632   tested strains (Six et al. 2021). The PE-rich strains show a much higher PUR/PAR ratio under

633   low cumulative diel photon doses during exponential phase, but decay towards a plateau and

634   reach a similar value to the PC-rich strains as cumulative diel photon dose increases. Thus the

635   PE-rich strains in exponential phase demonstrated higher ability to modulate light absorbance

636   capacity, whereas PC-rich strains retained a more stable PUR/PAR across cumulative diel

637   photon doses. What is more, during exponential phase, the PE-rich strains show a much higher

638   σ_{PSII}' under low cumulative diel photon dose, and their σ_{PSII}' remains higher than the PC-rich

639   strains, even as cumulative diel photon dose increases. Hence, PE-rich strains exhibit higher light

640 harvesting efficiency, at the expense of susceptibility to higher light levels, particularly under the

641 shortest (8h) and longest (24h) photoperiods.

642 *Synechococcus* exhibits remarkable acclimation within a strain to different environmental

643 conditions (Śliwińska-Wilczewska et al. 2018a, 2020; Aguilera et al. 2023). Under high

644 cumulative diel photon dose, *Synechococcus* employs photoprotective mechanisms to prevent the

645 harmful effects of excess light energy. These include the dissipation of excess energy as heat via

646 non-photochemical quenching (NPQ) and the regulation of phycobilisome antenna pigments, to

647 balance light absorption and energy transfer. In contrast, under conditions of low cumulative diel

648 PAR dose, *Synechococcus* sp. increases the expression of light-harvesting complexes to enhance

649 light absorption (Fig. 6) and capture (Fig. 7).

650 Available photic regimes, combining photoperiod and peak PAR, may determine the

651 occurrences of PC-rich and PE-rich picocyanobacterial phenotypes. Nitrogen (N) is an essential

652 element for cyanobacteria, while the N costs to produce photosynthetic pigments varies. The

653 molecular weight of the two phycoerythrin (PE; phycoerythrobilin) subunits is about 20,000 and

654 18,300 g mol^{-1}, while the two phycocyanin (PC; phycocyanobilin) subunits are about 17,600 and

655 16,300 g mol^{-1}, and allophycocyanin (APC) is lower still, about 16,000 g mol^{-1} (Bennett and

656 Bogorad 1971) and cell-specific content of this pigment is usually low in both phenotypes

657 (Śliwińska-Wilczewska et al. 2020). It follows that N-cost of producing PE is higher than that of

658 PC, even though PE-rich picocyanobacteria capture light better than PC-rich phenotypes (Fig. 6;

659 Fig. 7. Our results confirm that PE-rich strains are stronger light-harvesting competitors, while

660 the PC-rich strains have lower N-quotients for their phycobilin light capture system.

661

Photic regimes - implications for cumulative diel PSII electron flux

662

663   Algal dynamics respond rapidly to changes in environmental conditions (Connor 2018).

664 We used Fast Repetition Rate fluorometry (FRRf; Fig. 3) (Kolber et al. 1998) to generate an

665 index of PSII electron transport rate per unit volume (JV_{PSII}) (Oxborough et al. 2012; Tortell and

666 Suggett 2021; Berman-Frank et al. 2023), calibrated to absolute rates of electron transport

667 measured through oxygen evolution. Across different photic regimes the growth rates, μ, of PC-

668 rich and PE-rich picocyanobacteria show fairly consistent saturating responses to increasing

669 cumulative diel PSII electron flux (JV_{PSII}; µmol e$^-$ µmol Chl a^{-1} d^{-1}; Fig. 8). As previously found

670 for diatoms (Li et al. 2017) cumulative diel reductant generation was indeed a better predictor of

671 μ than was cumulative diel PUR, although photoperiod and peak PAR retain secondary

672 influences on achieved growth responses of the picocyanobacteria under some conditions.

673

Conclusions

674

675   Coastal picocyanobacteria show different growth responses to photoperiod and light level,

676 even under combinations giving equivalent cumulative diel PUR. Both PE-rich and PC-rich

677 strains of *Synechococcus* sp., grew fastest under moderate light and a 24 h photoperiod.

678 Consequently, *Synechococcus* sp. has the potential to emerge as components of the

679 phytoplankton during the Arctic or Antarctic summer under future, warmed, polar regions. In

680 optimal conditions (24 h of photoperiod and a peak PAR of 180 µmol photons m^{-2}s^{-1}), one of the

681 PE-rich *Synechococcus* sp., reached a chlorophyll-specific exponential growth rate of 4.5 d^{-1} (3.7

682 h doubling time), a record for a cyanobacteria. PE-rich strains in the exponential phase of growth

683 also demonstrated high ability to modulate their PUR/PAR ratio by adjusting pigment

684 composition, giving an advantage in the competition for light. We determined that growth yields

685   of PC-rich and PE-rich picocyanobacteria are well predicted by cumulative diel PSII electron

686   fluxes, across different photic regimes. PE-rich phenotypes of picocyanobacteria currently

687   predominate in abundance and genetic diversity in the Baltic Sea (Aguilera et al. 2023). This

688   dominance may be the result of eutrophication in the Baltic Sea, providing higher nitrogen for

689   phycobiliprotein synthesis, and leading to lower light even in near-surface waters. Our results

690   suggest possible expansion of the range of picocyanobacteria to new photic regimes in a warmed

691   future and indicate that PE-rich *Synechococcus* sp. may be a dominant component of

692   picophytoplankton in nutrient-rich environments.

693

694   **Additional Supporting Information may be found in the online version of this article.**

695

696   **Authors Contribution Statement:** S.S-W. designed the study with input from D.A.C. M.K.

697   estimated the transition point between exponential and pre-stationary phase of growth. M.S.

698   ensured the proper operation of the photobioreactors. A.A. conducted genetic analysis. N.M.O.

699   solved technical problems related to computer operation and software. S.S-W., M.S., N.M.O.,

700   D.A.C. contributed to R coding and data analysis. S.S-W. conducted the experiments, created

701   plots and wrote the manuscript, with support from D.A.C. All authors contributed to the

702   discussion of the results, supported manuscript preparation, and approved the final submitted

703   manuscript.

704

705   *Data availability statement*

706   Data supporting this study is available on:

707   https://github.com/FundyPhytoPhys/BalticPhotoperiod (public GitHub Repository) and

708 https://docs.google.com/spreadsheets/d/1ZXpwR7Gfto-

709 uRzVdXzMpQF4frbrvMLH_IyLqonFZRSw/edit#gid=0 (URL for MetaDataCatalog).

710   Code to perform data processing and analyses is available at

711 https://github.com/FundyPhytoPhys/BalticPhotoperiod.

712   16S rRNA sequences used in this study are available in GenBank under the accession

713 numbers PP034393, PP034394, PP034396 and PP034403.

714

721

Conflict of Interest

723 None declared.

724

References

726 Aguilera, A., J. Alegria Zufia, L. Bas Conn, and others. 2023. Ecophysiological analysis reveals

727 distinct environmental preferences in closely related Baltic Sea picocyanobacteria.

728 Environmental Microbiology **25**: 1674–1695. doi:10.1111/1462-2920.16384

729 Arrigo, K. R. 2014. Sea ice ecosystems. Annual Review of Marine Science **6**: 439–467.

730 doi:10.1146/annurev-marine-010213-135103

731 Beale, S. I. 1994. Biosynthesis of cyanobacterial tetrapyrrole pigments: Hemes, chlorophylls,

732 and phycobilins, p. 519–558. *In* D.A. Bryant [ed.], The Molecular Biology of Cyanobacteria.

733 Springer Netherlands.

734 Behrenfeld, M. J., R. T. O'Malley, D. A. Siegel, and others. 2006. Climate-driven trends in

735 contemporary ocean productivity. Nature **444**: 752–755. doi:10.1038/nature05317

736 Bennett, A., and L. Bogorad. 1971. Properties of subunits and aggregates of blue-green algal

737 biliproteins. Biochemistry **10**: 3625–3634. doi:10.1021/bi00795a022

738 Bennett, A., and L. Bogorad. 1973. Complementary Chromatic Adaptation in a filamentous blue-

739 green alga. Journal of Cell Biology **58**: 419–435. doi:10.1083/jcb.58.2.419

740 Berman-Frank, I., D. Campbell, A. Ciotti, and others. 2023. Application of Single Turnover

741 Active Chlorophyll Fluorescence for Phytoplankton Productivity Measurements. Version 2.0,

742 June, 26, 2023. Report Scientific Committee on Oceanic Research (SCOR) Working Group 156.

743 Boatman, T. G., R. J. Geider, and K. Oxborough. 2019. Improving the accuracy of Single

744 Turnover Active Fluorometry (STAF) for the estimation of Phytoplankton Primary Productivity

745 (PhytoPP). Frontiers in Marine Science **6**. doi:10.3389/fmars.2019.00319

746 Brand, L. E., and R. R. L. Guillard. 1981. The effects of continuous light and light intensity on

747 the reproduction rates of twenty-two species of marine phytoplankton. Journal of Experimental

748 Marine Biology and Ecology **50**: 119–132. doi:10.1016/0022-0981(81)90045-9

749   Chakdar, H., and S. Pabbi. 2016. Cyanobacterial phycobilins: Production, purification, and

750   regulation, p. 45–69. *In* P. Shukla [ed.], Frontier Discoveries and Innovations in Interdisciplinary

751   Microbiology. Springer India.

752   Christaki, U., S. Jacquet, J. R. Dolan, D. Vaulot, and F. Rassoulzadegan. 1999. Growth and

753   grazing on *Prochlorococcus* and *Synechococcus* by two marine ciliates. Limnology and

754   Oceanography **44**: 52–61. doi:10.4319/lo.1999.44.1.0052

755   Connor, D. 2018. Investigating the use of fast repetition rate fluorometry in understanding algal

756   physiology in optically complex oceans.

757   Elzhov, T. V., K. M. Mullen, A.-N. Spiess, and B. Bolker. 2023. Minpack.lm: R Interface to the

758   Levenberg-Marquardt Nonlinear Least-Squares Algorithm Found in MINPACK, Plus Support

759   for Bounds.

760   Erga, S. R., and B. R. Heimdal. 1984. Ecological studies on the phytoplankton of Korsfjorden,

761   western Norway. The dynamics of a spring bloom seen in relation to hydrographical conditions

762   and light regime. Journal of Plankton Research **6**: 67–90. doi:10.1093/plankt/6.1.67

763   Falkowski, P., and Z. Kolber. 1993. Estimation of phytoplankton photosynthesis by active

764   fluorescence. ICES Marine Science Symposium **197**: 92–103.

765   Field, C. B., M. J. Behrenfeld, J. T. Randerson, and P. Falkowski. 1998. Primary production of

766   the biosphere: Integrating terrestrial and oceanic components. Science **281**: 237–240.

767   doi:10.1126/science.281.5374.237

768 Flombaum, P., J. L. Gallegos, R. A. Gordillo, and others. 2013. Present and future global

769 distributions of the marine Cyanobacteria *Prochlorococcus* and *Synechococcus*. Proceedings of

770 the National Academy of Sciences **110**: 9824–9829. doi:10.1073/pnas.1307701110

771 Gradinger, R., and J. Lenz. 1989. Picocyanobacteria in the high Arctic. Marine Ecology Progress

772 Series **52**: 99–101. doi:10.3354/meps052099

773 Guillard, R. R. L. 1975. Culture of phytoplankton for feeding marine invertebrates, p. 29–60. *In*

774 W.L. Smith and M.H. Chanley [eds.], Culture of Marine Invertebrate Animals: Proceedings —

775 1st Conference on Culture of Marine Invertebrate Animals Greenport. Springer US.

776 Handel, A. 2020. Andreas Handel - Custom Word formatting using R Markdown.

777 Harrison, W. G., and T. Platt. 1986. Photosynthesis-irradiance relationships in polar and

778 temperate phytoplankton populations. Polar biology **5**: 153–164.

779 Haverkamp, T. H. A., D. Schouten, M. Doeleman, U. Wollenzien, J. Huisman, and L. J. Stal.

780 2009. Colorful microdiversity of *Synechococcus* strains (picocyanobacteria) isolated from the

781 Baltic Sea. The ISME Journal **3**: 397–408. doi:10.1038/ismej.2008.118

782 Hirata, T., N. J. Hardman-Mountford, R. J. W. Brewin, and others. 2011. Synoptic relationships

783 between surface Chlorophyll-*a* and diagnostic pigments specific to phytoplankton functional

784 types. Biogeosciences **8**: 311–327. doi:10.5194/bg-8-311-2011

785 Hoang, D. T., O. Chernomor, A. von Haeseler, B. Q. Minh, and L. S. Vinh. 2018. UFBoot2:

786 Improving the Ultrafast Bootstrap Approximation. Molecular Biology and Evolution **35**: 518–

787 522. doi:10.1093/molbev/msx281

788 Holtrop, T., J. Huisman, M. Stomp, and others. 2021. Vibrational modes of water predict spectral

789 niches for photosynthesis in lakes and oceans. Nature Ecology & Evolution **5**: 55–66.

790 doi:10.1038/s41559-020-01330-x

791 Huisman, J., M. Arrayás, U. Ebert, and B. Sommeijer. 2002. How do sinking phytoplankton

792 species manage to persist? The American Naturalist **159**: 245–254. doi:10.1086/338511

793 Jacob-Lopes, E., C. H. G. Scoparo, L. M. C. F. Lacerda, and T. T. Franco. 2009. Effect of light

794 cycles (night/day) on CO_2 fixation and biomass production by microalgae in photobioreactors.

795 Chemical Engineering and Processing: Process Intensification **48**: 306–310.

796 doi:10.1016/j.cep.2008.04.007

797 Jávorfi, T., J. Erostyák, J. Gál, A. Buzády, L. Menczel, G. Garab, and K. Razi Naqvi. 2006.

798 Quantitative spectrophotometry using integrating cavities. Journal of Photochemistry and

799 Photobiology B: Biology **82**: 127–131. doi:10.1016/j.jphotobiol.2005.10.002

800 Kalyaanamoorthy, S., B. Q. Minh, T. K. F. Wong, A. von Haeseler, and L. S. Jermiin. 2017.

801 ModelFinder: Fast model selection for accurate phylogenetic estimates. Nature Methods **14**:

802 587–589. doi:10.1038/nmeth.4285

803 Katoh, K., J. Rozewicki, and K. D. Yamada. 2019. MAFFT online service: Multiple sequence

804 alignment, interactive sequence choice and visualization. Briefings in Bioinformatics **20**: 1160–

805 1166. doi:10.1093/bib/bbx108

806 Klepacz-Smółka, A., D. Pietrzyk, R. Szeląg, P. Głuszcz, M. Daroch, J. Tang, and S. Ledakowicz.

807 2020. Effect of light colour and photoperiod on biomass growth and phycocyanin production by

808   *Synechococcus* PCC 6715. Bioresource Technology **313**: 123700.

809   doi:10.1016/j.biortech.2020.123700

810   Kolber, Z. S., O. Prášil, and P. G. Falkowski. 1998. Measurements of variable chlorophyll

811   fluorescence using fast repetition rate techniques: Defining methodology and experimental

812   protocols. Biochimica et Biophysica Acta (BBA) - Bioenergetics **1367**: 88–106.

813   doi:10.1016/S0005-2728(98)00135-2

814   Krishnan, A., M. Likhogrud, M. Cano, and others. 2021. *Picochlorum Celeri* as a model system

815   for robust outdoor algal growth in seawater. Scientific Reports **11**: 11649. doi:10.1038/s41598-

816   021-91106-5

817   Lane, D. J. 1991. 16S/23S rRNA sequencing. Nucleic acid techniques in bacterial systematics

818   115–175.

819   LaRoche, J., and B. M. Robicheau. 2022. The Pelagic Light-Dependent Microbiome, p. 395–

820   423. *In* L.J. Stal and M.S. Cretoiu [eds.], The Marine Microbiome. Springer International

821   Publishing.

822   Li, G., D. Talmy, and D. A. Campbell. 2017. Diatom growth responses to photoperiod and light

823   are predictable from diel reductant generation. Journal of Phycology **53**: 95–107.

824   doi:10.1111/jpy.12483

825   Li, Q., L. Legendre, and N. Jiao. 2015. Phytoplankton responses to nitrogen and iron limitation

826   in the tropical and subtropical Pacific Ocean. Journal of Plankton Research **37**: 306–319.

827   doi:10.1093/plankt/fbv008

828   Li, W. K. W. 1995. Composition of ultraphytoplankton in the central North Atlantic. Marine

829   Ecology Progress Series **122**: 1–8.

830   Ligges, U., T. Short, P. Kienzle, and others. 2024. Signal: Signal Processing.

831   Litchman, E., C. A. Klausmeier, and K. Yoshiyama. 2009. Contrasting size evolution in marine

832   and freshwater diatoms. Proceedings of the National Academy of Sciences **106**: 2665–2670.

833   doi:10.1073/pnas.0810891106

834   Longobardi, L., L. Dubroca, F. Margiotta, D. Sarno, and A. Zingone. 2022. Photoperiod-driven

835   rhythms reveal multi-decadal stability of phytoplankton communities in a highly fluctuating

836   coastal environment. Scientific Reports **12**: 3908. doi:10.1038/s41598-022-07009-6

837   MacIntyre, H. L., T. M. Kana, R. J. Geider, H. L. MacIntyre, T. M. Kana, and R. J. Geider. 2000.

838   The effect of water motion on short-term rates of photosynthesis by marine phytoplankton.

839   Trends in Plant Science **5**: 12–17. doi:10.1016/S1360-1385(99)01504-6

840   Moejes, F. W., A. Matuszyńska, K. Adhikari, and others. 2017. A systems-wide understanding

841   of photosynthetic acclimation in algae and higher plants. Journal of Experimental Botany **68**:

842   2667–2681. doi:10.1093/jxb/erx137

843   Morel, A. 1978. Available, usable, and stored radiant energy in relation to marine

844   photosynthesis. Deep Sea Research **25**: 673–688. doi:10.1016/0146-6291(78)90623-9

845   Morel, A. 1988. Optical modeling of the upper ocean in relation to its biogenous matter content

846   (case I waters). Journal of Geophysical Research: Oceans **93**: 10749–10768.

847   doi:10.1029/JC093iC09p10749

848   Oxborough, K., and N. R. Baker. 1997. Resolving chlorophyll *a* fluorescence images of

849   photosynthetic efficiency into photochemical and non-photochemical components – calculation

850   of qP and Fv-/Fm-; without measuring Fo-; Photosynthesis Research **54**: 135–142.

851   doi:10.1023/A:1005936823310

852   Oxborough, K., C. M. Moore, D. J. Suggett, T. Lawson, H. G. Chan, and R. J. Geider. 2012.

853   Direct estimation of functional PSII reaction center concentration and PSII electron flux on a

854   volume basis: A new approach to the analysis of Fast Repetition Rate fluorometry (FRRf) data.

855   Limnology and Oceanography: Methods **10**: 142–154. doi:10.4319/lom.2012.10.142

856   Pedersen, T. L. 2024. Patchwork: The Composer of Plots.

857   Pick, F. R. 1991. The abundance and composition of freshwater picocyanobacteria in relation to

858   light penetration. Limnology and Oceanography **36**: 1457–1462. doi:10.4319/lo.1991.36.7.1457

859   Posit team. 2022. RStudio: Integrated development environment for r, Posit Software, PBC.

860   R Core Team. 2023. R: A language and environment for statistical computing, R Foundation for

861   Statistical Computing.

862   Reynolds, C. S. 2006. The Ecology of Phytoplankton, Cambridge University Press.

863   Ryan, J. A., J. M. Ulrich, R. Bennett, and C. Joy. 2024. Xts: eXtensible Time Series.

864   Sakamoto, T., and D. A. Bryant. 1999. Nitrate transport and not photoinhibition limits growth of

865   the freshwater cyanobacterium *Synechococcus* species PCC 6301 at low temperature. Plant

866   Physiology **119**: 785–794. doi:10.1104/pp.119.2.785

867   Schuurmans, R. M., J. C. P. Matthijs, and K. J. Hellingwerf. 2017. Transition from exponential

868   to linear photoautotrophic growth changes the physiology of *Synechocystis* sp. PCC 6803.

869   Photosynthesis Research **132**: 69–82. doi:10.1007/s11120-016-0329-8

870   Serway, R. A., C. J. Moses, and C. A. Moyer. 2004. Modern Physics, Cengage Learning.

871   Six, C., Z. V. Finkel, A. J. Irwin, and D. A. Campbell. 2007. Light variability illuminates niche-

872   partitioning among marine picocyanobacteria. PLOS ONE **2**: e1341.

873   doi:10.1371/journal.pone.0001341

874   Six, C., M. Ratin, D. Marie, and E. Corre. 2021. Marine *Synechococcus* picocyanobacteria: Light

875   utilization across latitudes. Proceedings of the National Academy of Sciences **118**: e2111300118.

876   doi:10.1073/pnas.2111300118

877   Śliwińska-Wilczewska, S., A. Cieszyńska, J. Maculewicz, and A. Latała. 2018a.

878   Ecophysiological characteristics of red, green, and brown strains of the Baltic

879   picocyanobacterium *Synechococcus* sp. – a laboratory study. Biogeosciences **15**: 6257–6276.

880   doi:10.5194/bg-15-6257-2018

881   Śliwińska-Wilczewska, S., Z. Konarzewska, K. Wiśniewska, and M. Konik. 2020.

882   Photosynthetic pigments changes of three phenotypes of picocyanobacteria *Synechococcus* sp.

883   Under different light and temperature conditions. Cells **9**: 2030. doi:10.3390/cells9092030

884   Śliwińska-Wilczewska, S., J. Maculewicz, A. Barreiro Felpeto, and A. Latała. 2018b.

885   Allelopathic and bloom-forming picocyanobacteria in a changing world. Toxins **10**: 48.

886   doi:10.3390/toxins10010048

887 Stadnichuk, I. N., P. M. Krasilnikov, and D. V. Zlenko. 2015. Cyanobacterial phycobilisomes

888 and phycobiliproteins. Microbiology **84**: 101–111. doi:10.1134/S0026261715020150

889 Stomp, M., J. Huisman, L. Vörös, F. R. Pick, M. Laamanen, T. Haverkamp, and L. J. Stal. 2007.

890 Colourful coexistence of red and green picocyanobacteria in lakes and seas. Ecology Letters **10**:

891 290–298. doi:10.1111/j.1461-0248.2007.01026.x

892 Strickland, J. D., and T. R. Parsons. 1972. Practical Hand Book of Seawater Analysis. Fisheries

893 Research Board of Canada **167 (2nd edition)**: 1–311. doi:DOI: http://dx.doi.org/10.25607/OBP-

894 1791

895 Theus, M. E., T. J. Layden, N. McWilliams, S. Crafton-Tempel, C. T. Kremer, and S. B. Fey.

896 2022. Photoperiod influences the shape and scaling of freshwater phytoplankton responses to

897 light and temperature. Oikos **2022**: e08839. doi:10.1111/oik.08839

898 Torremorell, A., M. E. Llames, G. L. Pérez, R. Escaray, J. Bustingorry, and H. Zagarese. 2009.

899 Annual patterns of phytoplankton density and primary production in a large, shallow lake: The

900 central role of light. Freshwater Biology **54**: 437–449. doi:10.1111/j.1365-2427.2008.02119.x

901 Tortell, P., and D. J. Suggett. 2021. A user guide for the application of Single Turnover active

902 chlorophyll fluorescence for phytoplankton productivity measurements. Version 1. Report

903 Scientific Committee on Oceanic Research (SCOR) Working Group 156.

904 van Alphen, P., H. Abedini Najafabadi, F. Branco dos Santos, and K. J. Hellingwerf. 2018.

905 Increasing the photoautotrophic growth rate of *Synechocystis* sp. PCC 6803 by identifying the

906 limitations of its cultivation. Biotechnology Journal **13**: 1700764. doi:10.1002/biot.201700764

907   Velichko, N., S. Smirnova, S. Averina, and A. Pinevich. 2021. A survey of Antarctic

908   cyanobacteria. Hydrobiologia **848**: 2627–2653.

909   Vincent, W. F., J. P. Bowman, L. M. Rankin, and T. A. McMeekin. 2000. Phylogenetic diversity

910   of picocyanobacteria in Arctic and Antarctic ecosystems. Microbial biosystems: new frontiers.

911   Proceedings of the 8th International Symposium on Microbial Ecology 317–322.

912   Wickham, H. 2016. Data Analysis, p. 189–201. *In* H. Wickham [ed.], Ggplot2: Elegant Graphics

913   for Data Analysis. Springer International Publishing.

914   Wood, S. N. 2017. Generalized Additive Models: An Introduction with R, Second Edition, 2nd

915   ed. Chapman and Hall/CRC.

916   Xi, H., S. N. Losa, A. Mangin, and others. 2020. Global retrieval of phytoplankton functional

917   types based on empirical orthogonal functions using CMEMS GlobColour merged products and

918   further extension to OLCI data. Remote Sensing of Environment **240**: 111704.

919   doi:10.1016/j.rse.2020.111704

920   Xu, K., J. L. Grant-Burt, N. Donaher, and D. A. Campbell. 2017. Connectivity among

921   Photosystem II centers in phytoplankters: Patterns and responses. Biochimica et Biophysica Acta

922   (BBA) - Bioenergetics **1858**: 459–474. doi:10.1016/j.bbabio.2017.03.003

923   Xu, K., J. Lavaud, R. Perkins, E. Austen, M. Bonnanfant, and D. A. Campbell. 2018.

924   Phytoplankton σPSII and excitation dissipation; implications for estimates of primary

925   productivity. Frontiers in Marine Science **5**. doi:10.3389/fmars.2018.00281